https://doi.org/10.5194/essd-2026-501
Preprint. Discussion started: 22 July 2026

Synoptic hydrographic monitoring across the Kongsfjorden–Krossfjorden system and the Fram Strait: five-year time series from the Italian Arctic Marine Observing System

Francesco Paladini de Mendoza[1], Leonardo Langone[2], Alice Cavaliere[2], Gianmarco Ingrosso[3], Lorenzo Pasculli[4], Chiara Ripa[5], Mauro Mazzola[2], Manuel Bensi[4], Federico Giglio[2], Stefano Miserocchi[2], Tommaso Tesi[2], Patrizia Giordano[2]

[1] Institute of Polar Science (ISP), National Research Council (CNR), Messina, 98122, Italy
[2] Institute of Polar Science (ISP), National Research Council (CNR), Bologna, 40129, Italy
[3] Institute of Research on Terrestrial Ecosystems (IRET), National Research Council (CNR), Lecce, 73100, Italy
[4] Oceanographic Section, National Institute of Oceanography and Applied Geophysics - OGS, Sgonico, 34010, Italy
[5] Institute of Polar Science (ISP), National Research Council (CNR), Roma, 00015, Italy

Correspondence to: Francesco Paladini de Mendoza (francesco.paladinidemendoza@cnr.it)

Abstract. Arctic fjords represent highly dynamic interfaces between the open ocean, the cryosphere, and terrestrial freshwater sources, where climate driven changes in heat, freshwater, and circulation are rapidly emerging. Here we present a five-year (2020–2025) oceanographic dataset from the Italian Arctic Marine Observing System, providing continuous moored observations across the Kongsfjorden–Krossfjorden fjord system and offshore the South Cape in the eastern Fram Strait off Svalbard. The marine observing system integrates four mooring sites with different hydrographic properties, delivering high-resolution time series of temperature, salinity, and ocean current both in the fjord, on the continental shelf and along the continental slope. The dataset is fully quality controlled following standardized procedures, ensuring long-term comparability across deployments. Thermohaline properties are used to classify water masses and characterize seasonal to interannual variability. The observations reveal contrasting regimes, with relatively stable deepwater offshore conditions and highly variable fjord environments governed by atmospheric forcing, freshwater input from glaciers, and shelf–fjord exchange processes. Episodic intrusions of Atlantic origin waters are detected at both fjord entrance and inner fjord sites, providing direct observational evidence of Atlantification processes. Owing to its temporal resolution, vertical coverage, and spatial distribution, the dataset supports a broad range of scientific and operational applications. The dataset is openly available through the Italian Arctic Data Center and fully compliant with FAIR (Findable, Accessible, Interoperable and Reusable) principles, contributing to sustained Arctic observing efforts and long-term assessments of Arctic–Atlantic interactions relevant to Arctic Ocean circulation and the Atlantic Meridional Overturning Circulation.

https://doi.org/10.5194/essd-2026-501
Preprint. Discussion started: 22 July 2026

1 Introduction

Polar regions are rapidly warming (Chylek et al., 2009; Serreze & Barry, 2011; Richter-Menge & Druckenmiller, 2019), driving major physical changes in the ocean, sea ice loss (Comiso, 2012; Carmack et al., 2015) and ecosystems impacts. In the Arctic these shifts influence the world ocean circulation with a key role on the deep-water formation within the Atlantic Meridional Overturning Circulation (Carmack & Aagaard, 1973; Killworth, 1983; Rudels, 1995; Tanhua et al., 2005), through modifications of deep-water formation and the exchange of heat, salt, and nutrients between the Arctic and Atlantic Ocean. The Fram Strait, between Greenland and Svalbard, is the main gateway where warm Atlantic waters entering in the Nordic seas and cold Arctic Waters returns southward. Recent intensification of Atlantic Water inflow has produced a marked "Atlantification" (Polyakov et al., 2017; Lind et al., 2018), especially in the Eurasian Arctic region and Svalbard Archipelago, altering stratification, sea ice cover and air-sea interactions (Ingvaldsen et al., 2021).

Svalbard's western shelves are characterized by the interplay between the West Spitsbergen Current (WSC), a branch of the North Atlantic Current (Teigen et al., 2011) and the colder Spitsbergen Polar Current (SPC) combined with glacial meltwaters and river discharges, sea ice processes and local atmospheric circulation (Cottier et al., 2007; Stigebrandt, 2012; De Rovere et al., 2025). WSC transport warm, saline, nutrient rich waters and is characterized by significant seasonal and interannual variability (Muilwijk et al., 2018; Wang et al., 2021; Bensi et al., 2019, 2025). In contrast, the SPC, derived from the East Spitsbergen Current (ESC), carries Arctic Waters (ArW) (Nielsen et al., 2021; Bensi et al., 2025) and sea ice (Tverberg et al., 2019) bounding the West Spitsbergen Shelf. The Atlantic Waters intrusion inside the fjord are caused by synergic interaction between offshore hydrological conditions over the continental shelf and local atmospheric forcing (Skogseth et al., 2020; De Rovere et al., 2022). Enhanced glacier melting and landscape changes further modify particulate delivery and biogeochemical conditions in coastal waters (Ingrosso et al., 2025).

To monitoring Essential Ocean Variables (EOV) across different time scales (from seasonal to multi-annual), the Italian contribution to the Atlantic-Arctic Distributed Biological Observatory (A-DBO) and to Svalbard Integrated Earth Observing System (SIOS) established a marine network of moorings beginning with the "Mooring Dirigibile Italia" (MDI) in Konsfjorden started in 2010 (Aliani et al., 2016; D'Angelo et al., 2018; De Rovere et al., 2022; Nicolai et al., 2025). The system expanded in 2014 with moorings located in the Fram Strait (S1, ID2), along the continental slope on the south-western edge of Spitsbergen (Bensi et al., 2019) and additional moorings in the Kongsfjorden–Krossfjorden system (KIM, MAP, see Figure 1), since 2020, to investigate fjord–shelf exchanges and the influence of tidewater versus land-terminating glaciers. Tidewater glaciers, which interact directly with the ocean, are particularly sensitive to heat exchange, which in turn affect the stability of inland ice. In contrast, land-terminating glaciers are more influenced by atmospheric dynamics, and their retreat is associated with key environmental feedback such as the vegetation coverage expansion in previously ice-covered soils and the release of greenhouse gases from the degradation of formerly frozen organic matter. The mooring KIM was positioned near the entrance of Krossfjorden, an area more exposed to oceanic processes. Collectively, these moorings document ocean processes of the Svalbard region (Bensi et al., 2025) and contribute to fjord-shelf exchanges analysis (De Rovere et al., 2024,

https://doi.org/10.5194/essd-2026-501
Preprint. Discussion started: 22 July 2026

2025). The quality assurance (QA) and quality control (QC) of data acquired are crucial for reliability of the dataset produced to determine the level of accuracy of the observed fluctuations at different temporal scales. Monitoring program was accompanied by the development of Digital Infrastructure (DI) designed to collect, manage, and publish the results of scientific research conducted in the Arctic region fully compliant with FAIR principles (Findable, Accessible, Interoperable and Reusable, Wilkinson et al., 2016; Tanhua et al., 2019).

This study focuses on observations from the distributed Italian Arctic Marine Observing system over the past five years (2020–2025), examining thermohaline and hydrodynamic data collected from moorings. It also describes the data flow management system used for storing information in the Italian Arctic Data Center, which is integrated with international Arctic observing programmes. Robust QA/QC data acquisition and FAIR-compliant data management support understanding and decision-making strategies related to ongoing Arctic environmental change, contributing critically to the Arctic observing system community.

2 Mooring sites overview

Data presented in this study were acquired by four moorings located in different sites of the Svalbard region (Figure 1a). The mooring lines (Figure 1c) are equipped with a series of different sensors and devices to characterise both physical and biogeochemical parameters (e.g., time-series sediment traps and biogeochemistry sensors). In this study we focus exclusively on temperature, salinity and current data using data collected between 2020 and 2025. The moorings were deployed at four distinct locations characterised by constrasting geomorphological and oceanographic settings:

- Mooring MDI and MAP are both located in Kongsfjorden, at 100 and 40 m depth, respectively, in two different positions along the fjord axis (Figure 1b). MDI (78°58.8'N, 12°14.1'E) is placed in the inner part of the fjord in front of the Kronebreen- Kongsvegen tidewater glacier system; MAP (78°56.6'N, 11°52.7'E) is placed in front of the Bayelva river mouth, which drains waters from the land-terminating Brøggerbreen glacier (Repp, 1988).
- The mooring KIM is placed in Krossfjorden, a north-south oriented fjord that converges together with Kongsfjorden submarine channel in the deep glacial basin, the Kongsfjordrenna (Figure 1b). The mooring location is 79°07.6'N, 11°43.4'E, in the mid-right side of the fjord at 300 m depth closer to the fjord entrance. Although the area is strongly influenced by the presence of tidewater glaciers (Svendsen et al., 2002), the mooring is under the influence of the up-fjord flow currents that flow northward along the Spitsbergen shelf (Svendsen et al., 2002).
- The mooring S1 is located southwest of the South Cape of the Svalbard Islands (76°26.2'N, 13°56.9'E, Figure 1a) at about 1040 meter depth (Bensi et al., 2019; 2020; 2025; Szesciorka et al., 2025) on the eastern side of the Fram Strait. This region is strongly influenced by the interaction of different water masses including i) the northward-moving Atlantic Waters (AW), which lie in the upper-intermediate layers, ii) the Norwegian Sea Deep Water (NSDW), which lies below 900 m depth (Walczowski et al., 2005; Wobus et al., 2013; Bensi et al., 2019), and iii) the

Polar and ice-melting waters coming from fjords (e.g., Hornsund, Storfjorden) and from the eastern part of the Svalbard archipelago (Eriksen et al, 2018).

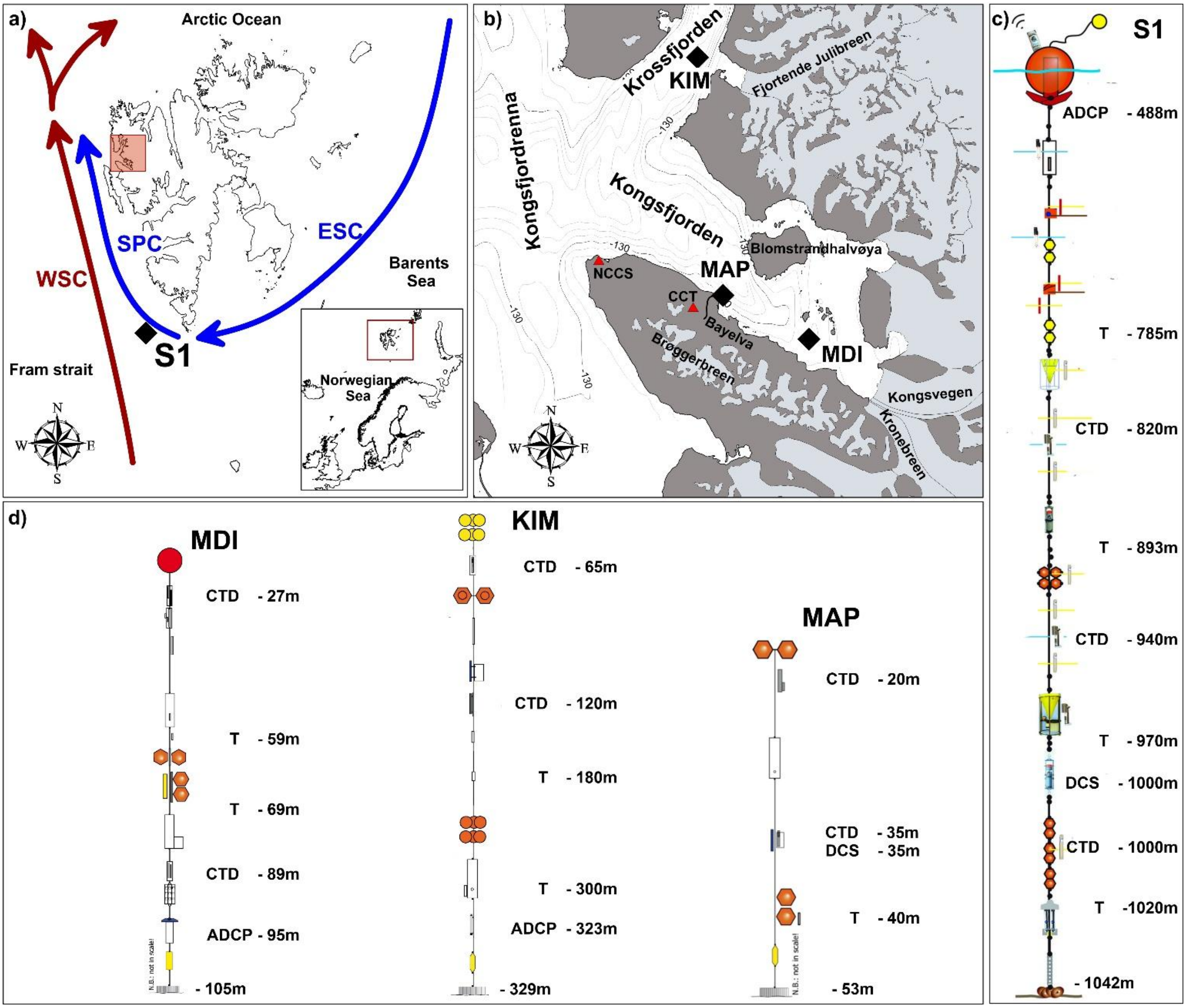

Figure 1: Study sites: location of the Italian Arctic Marine Observing system in the Svalbard Archipelago (a); b) detail of Kongsfjorden-Krossfjorden system, where MAP, MDI and KIM moorings are located; in the map are reported also the meteorological stations located at NyAlesund (Climate Change Tower -CCT) and in Kvdehuken (Norwegian Centre for Climate Services, NCCS); c) offshore deep-water S1 mooring sketch; d) coastal infjord mooring sketches (MDI, KIM, MAP); In the sketches there are details about mooring ballast depth, Acoustic Doppler Current Profiler (ADCP) and Conductivity-Temperature-Depth (CTD) position throughout the water column and are reported only the sensors presented in this work

Oceanographic moorings are configured and maintained for continuous long-term monitoring following the management approach used in EMSO-ERIC observatory (Coppola et al., 2016; Pearlman et al., 2019; Paladini de Mendoza et al., 2022).

https://doi.org/10.5194/essd-2026-501
Preprint. Discussion started: 22 July 2026

Open Access Earth System Science Data Discussions

The resulting dataset presented here covers the period from September 2020 to July 2025 for all moorings, except for S1, whose data extend only until July 2024 due to technical problems occurred in 2025. Details about surveys are reported in Table 1 where there is the general description about the temporal extensions of each measuring period, the mooring location, depth, and models of the ADCP and CTD systems used.

	Mooring MDI					
N°	**start (DDMMYY)**	**End (DDMMYY)**	**Mooring position (Lat N, Lon E)**	**Depth (m below the sea surface)**	**current meter type (depth)**	**CTD type (m below the sea surface)**
1	12/09/20	01/09/21	78°54.875'N 12°14.178'E	105	-	SBE56 (59m) SBE56 (69m) SBE16 (89m)
2	13/09/21	30/08/22	78°54.866'N 12°14.270'E	104	ADCP (95m)	SBE16 (27m) SBE56 (59m) SBE56 (69m) SBE16 (89m)
3	15/09/22	28/08/23	78°54.870'N 12°14.206'E	105	ADCP (95m)	SBE16 (27m) SBE56 (59m) SBE56 (69m) SBE16 (89m)
4	09/09/23	31/08/24	78°54.868'N 12°14.153'E	105	ADCP (95m)	SBE16 (27m) SBE56 (59m) SBE56 (69m) SBE37 (89m)
5	11/09/24	12/06/25	78°55.126'N 12°13.700'E	107	ADCP (95m)	SBE16 (27m) SBE56 (59m) SBE56 (69m) SBE37 (89m)
	Mooring MAP					
1	11/09/20	01/09/21	78°56.67'N 11°52.71'E	46	DCS (35m)	SBE37 (35m)
2	18/09/21	30/08/22	78°56.600'N 11°52.671'E	43	DCS (35m)	SBE37 (20m), SBE37 (35m), SBE56 (40m)
3	05/09/22	29/08/23	78°56.589'N 11°52.655'E	43	DCS (35m)	SBE37 (20m), SBE37 (35m), SBE56 (40m)
4	11/09/23	31/08/24	78°56.698'N 11°52.856'E	53	DCS (35m)	SBE37 (20m), SBE37 (35m), SBE56 (40m)
5	11/09/24	12/06/25	78°56.521'N 11°52.824'E	97	DCS (35m)	SBE37 (20m), SBE37 (35m), SBE56 (40m)
	Mooring KIM					
1	08/03/20	21/06/21	79°07.648'N 11°43.446'E	320	-	SBE56 (65m) SBE16 (120m) SBE56 (180m)

https://doi.org/10.5194/essd-2026-501
Preprint. Discussion started: 22 July 2026

2	29/06/21	06/11/22	79°07.620'N 11°43.460'E	320	-	SBE56 (65m) SBE16 (120m) SBE56 (180m)
3	13/12/22	18/04/23	79°07.627'N 11°43.493'E	320	-	SBE37 (65m) SBE37 (120m) SBE56 (180m) SBE56 (300m)
4	18/04/23	08/11/24	79°07.678'N 11°43.422'E	329	ADCP (323m)	SBE37 (180m) SBE16 (239m) SBE56 (300m)
5	09/11/24	09/03/25	79°07.627'N 11°43.493'E	326	-	SBE37 (65m) SBE16 (120m) SBE56 (180m) SBE56 (300m)
	Mooring S1					
1	31/10/19	31/08/21	76°26.73'N 13°56.44'E	1038	ADCP (780m), DCS (1000m)	SBE37 (785m) SBE37 (820m) SBE56 (893m) SBE56 (970m) SBE16 (1000m) SBE56 (1020)
2	01/09/21	11/06/22	76°26.28'N 13°56.93'E	1042	ADCP (740m), DCS (1000m)	SBE56 (785m) SBE37 (820m) SBE56 (893m) SBE37 (940m) SBE16 (1000m) SBE56 (1020)
3	25/06/22	22/06/23	76°26.29'N 13°57.05'E	1042	ADCP (488m), DCS (1000m)	SBE56 (785m) SBE37 (820m) SBE56 (893m) SBE37 (940m) SBE56 (970m) SBE16 (1000m) SBE56 (1020)
4	07/07/23	04/07/24	76°26.29'N 13°57.05'E	1042	-	SBE56 (785m) SBE37 (820m) SBE56 (893m) SBE37 (940m) SBE16 (1000m) SBE56 (1020)

Table 1: Survey details on the four mooring sites with start and end of each survey; mooring position (Lat, Lon); depth of mooring site; current meter type used (Acoustic Doppler Current Profiler, ADCP and Doppler Current Sensor, DCS) and its deployment depth; CTD type used and its deployment depth.

3 Observatory scheme and long-term practice of mooring maintenance in the extreme environment

The maintenance phase of each deployment includes a CTD cast at the mooring site before recovery/deployment, data download, battery replacement, sensor check, and cleaning and verification of all components (ropes, shackles and hooks) to ensure proper functioning, for the next acquisition cycle. Serial numbers are tracked to document sensor replacement.

CTD probes along the mooring line continuously record temperature, conductivity, and pressure. Two Sea-Bird models are used: SBE 16plus V2 SeaCAT and SBE37SMP-ODO. Measurements span 2020-2025 and are organised in annual deployments. Most probes acquire data every 30 - 60 minutes, except the SBE 16plus at 27 m depth on MDI, set to 3-hour intervals to extend battery life while co-operating with other sensors. The SBE 16plus V2 SeaCAT includes a pump for antifouling and offers high-accuracy temperature, conductivity, and pressure data. The SBE37SMP-ODO, also equipped with pump and antifouling tablets, provides comparable accuracy for long-term deployments.

All CTDs undergo factory calibration (Sea-Bird Europe - European Calibration and Repair Center) and annual pre- and post-deployment CTD profiles for comparison carried out with a calibrated SBE19plus, used as reference for quality control.

https://doi.org/10.5194/essd-2026-501
Preprint. Discussion started: 22 July 2026

Two types of current meters are used: single point acoustic meters and ADCPs. Single-point systems include the Aquadopp 2 MHz (MAP mooring, 2020-2025) and the Aanderaa RCM-Seaguard (S1 mooring, 1000 m depth). Both kind of instruments measure current speed and direction in a single cell with 0.5m blanking distance and are equipped with tilt, compass, thermistor and pressure sensors. The Aquadopp samples at 1 Hz (averaged over 60 s recorded every 1800 s) while the Aanderaa collects 600 pings every 60 minutes. Compass calibration is repeated before each deployment.

ADCPs include Teledyne RDI and Nortek Signature systems. At MDI, a Sentinel V 100 (300 kHz, 5-beam, 20°), is deployed upward-looking at ~95 m, with 90 cells of 1 m and hourly measurements (300 s ensemble). At S1, a Quartermaster (150 kHz, 4 beams, 20°) operated downward looking at ~740 m during the 2021- 2022 deployment and at ~ 488 m depth during the 2022 - 2023 deployment with 32 cells of 8 m and 30 minutes sampling interval. At KIM, a Nortek Signature 250 (250 kHz, 4-beam, 20°) works upward-looking at 323 m, with 27 cells of 8 m and 2-hours interval.

All ADCPs compute sound speed from assumed salinity and transducer depth and measure temperature via internal thermistor. Magnetic declination corrections are applied during processing due to significant Arctic deviation between magnetic and geographical North, which is significant at the Arctic latitudes. In the Kongsfjordrenna (79.03°N, 11.27°E), declination was 7.33°E in 2020, increasing 0.45°/yr, while at S1 (76.43°N, 13.95°E) it was 8.47°E changing by 0.38°/yr. The magnetic declination values were obtained from the NOAA Magnetic Field Calculators (National Centers for Environmental Information; https://www.ngdc.noaa.gov/geomag/calculators/magcalc.shtml#bearing; last access 12/09/2025).

4 Quality Control and Data Flow Management

The data flow management of the Italian Marine Observing System follows a step-by-step procedure that starts with a visual check of the hydrodynamic and thermohaline data acquired after the mooring recovery. During this phase, a general check is conducted to ensure the correct functioning of the instrumentation, deployment depth, and the start and end of the acquisition, noting any malfunctions that may have occurred. In addition, a preliminary check of the data quality is obtained evaluating the average values of the parameter measured and the overall 'noisiness' of the plot. One key parameter for the first screening phase is the pressure sensor depth, which indicates the actual operating depth, and the deployment and recovering phase. In this way all records during deployment and recovery phase are filtered out, in the whole dataset a minimum of 0.1% and maximum of 1.3% of data were removed from the dataset.

4.1 Thermohaline data

The Quality Control (QC) procedure applied to the thermohaline and hydrodynamic data referred to the methodology applied in Paladini de Mendoza et al. (2022) with some improvement detailed below. For CTD measurements, the raw hexadecimal data were converted to ASCII by the SBE Data Processing™ and the QC procedure added a time and pressure check. Regarding time any anomalies such as no sequential time steps and spurious values were detected and flagged. Regarding the pressure sensor (when present) the values are screened detecting presence of negative values and values outside a defined range of the correct position, defined as 10 meters above and below a reference depth determined after the check that deployment depth

https://doi.org/10.5194/essd-2026-501
Preprint. Discussion started: 22 July 2026

design agrees with the actual depth of the sensor. After, the Spike and Gradient test are applied and regarding Gradient Test (GT) a new implementation is developed for the threshold used to flag bad data. The GT is evaluated if the gradient between adjacent salinity and temperature measurements are too steep, and the gradient threshold is set as 50% of the data range.

4.2 Ocean current data

For the ADCP data, the QC procedure follows the methodology described in Paladini de Mendoza et al. (2022) with additional improvements implemented including time and pressure consistency checks applied on the assumption outlined in the previous "thermohaline data" section. Pitch and roll values are also examined and observations exceeding 20° are flagged since such tilts compromise the correct cell-depth determination. This procedure proved essential for identifying anomalies such as those occurring at the MDI site during 2022-2023 deployment, when the ADCP became entangled with the mooring line, tilted beyond 20°, and produced unusable data (resulting in the gap shown in Figure 2b). Once QC calculations are completed, the time-series is organized so that each observation is accompanied by a SeaDataNet qualifier flag, assigned following the SeaDataNet QC guidelines (SeaDataNet, 2010) and the L20 SeaDataNet Measurand Qualifier flags (last updated at http://seadatanet.maris2.nl/v_bodc_vocab_v2/browse.asp?order=conceptid&formname=search&screen=0&lib=l20). The archived dataset includes all records, with data quality expressed exclusively through these qualifier flags without modifying the original records. Main QC codes used are data that passed all QC tests, flagged with code 1, data that failed at least one test, flagged with code 4, and missing data, flagged with code 9. All data collected during the deployment and recovery phases were excluded from the final dataset because the instrument did not operate at the planned acquisition depths defined by the mooring-line configuration.

5 Data Analysis

The five-year mooring data are analysed with standardised analysis applied to compare measurements conducted in each mooring site. Temperature and Salinity data are further processed to obtain Conservative Temperature (CT, °C) and Absolute Salinity (S_A, g/kg), respectively. CT, S_A and Density Anomaly (σ_θ) are calculated using the Thermodynamic Equation of Seawater - 2010 (TEOS-10) and the GSW Oceanographic Toolbox equations (Jackett, et al., 2006; IOC, SCOR and IAPSO, 2010; McDougall and Barker, 2011; McDougall et al., 2012). Daily and monthly mean values are calculated from the original data (e.g., temporal resolution from 30 min to 3 hours). For hydrodynamic records acquired with ADCP, temporal and spatial variability are observed considering three depths along the water column (roughly to 1/3 of the measured water column for nearshore) and approximately every 100 m on the offshore mooring. In contrast, single point current meters provide measurements at a single water depth. The overview of the current field is obtained by building a polar histogram with directions binned every 5° and speed grouped into three classes. Monthly and seasonal patterns of thermohaline and hydrodynamic data are calculated and compared between years to give an intra- and inter-annual overview of the variability.
Fieldwork procedures and instrumentation management routines, developed and refined over the years, are designed to ensure quality assurance (QA) of data acquisition. Together with the QC procedures and data management practices described in the

https://doi.org/10.5194/essd-2026-501
Preprint. Discussion started: 22 July 2026

following section, they support and move toward the Transparency, Responsibility, User focus, Sustainability and Technology principles, (TRUST, Lin et al., 2020) of digital repository.

6 Metadata and Italian Arctic Data Center (IADC) Dataset Archive

The dataset is organized in NetCDF files produced for each sensor and for each deployment phase (usually about one year long). The NetCDF file is built starting from the NCEI NetCDF Templates of NOAA that allow data producers to create netCDF datasets that conform to Unidata's Attribute Convention for Dataset Discovery (ACDD) and Climate and Forecast (CF) Conventions. The basic structure provided by NCEI is modified following the OceanSITES Data Format (OceanSITES, 2020) and EMSO-ERIC (European Seafloor and water-column Observatory), which are reference standards for European oceanographic and fixed marine observatories. Attribute metadata are standardised using controlled vocabularies from the NERC Vocabulary Service. The metadata describing the records are divided in generic attributes and data attributes. The global attributes give a generic description of the dataset framing the platform (L06, SeaVoX Platform Categories), institution (EDMO code) providing the data, the spatial (geographical coordinates and C19 code, SeaVoX salt and fresh water body gazetteer) and temporal coverage together with contact of principal investigator and the description of the discipline regarding the dataset (P08), the collected parameters (P03) and the instrument used all codified by SeaDataNet vocabularies (i.e P02, L05). In addition, also the licence type applied to the data and the funding source is specified following Creative Common categories. The data attributes give specific information on the sensor used (model, L22, and manufacturer, L35), the parameter name (P01) and the measurement unit (P06). The datasets are stored on the IADC (Italian Arctic Data Center) that follows the ERDDAP (Environmental Research Division's Data Access Program) protocol explained in detail in the next section.

6.1 IADC Data Portal

The IADC is a Digital Infrastructure (DI) designed to collect, manage, and publish the results of scientific research conducted in the Arctic region within the framework of the Climate Change Tower Integrated Project (CCT-IP) and other initiatives carried out by Italian research institutions (INAF, OGS, CNR, ENEA, INGV) and universities (Infrastrutture di ricerca e siti osservativi, Rapporto annuale 2023). The DI provides multiple functions such as an automated data acquisition system that gathers real-time measurements from Svalbard (i.e. Amundsen-Nobile Climate Change Tower; Mazzola et al., 2016) with autonomous routine and from the instruments installed on moorings through manual procedure. It also includes a metadata catalogue for documenting research activities and a data repository for managing research data. The metadata are managed through GeoNetwork, an open-source catalog application designed for managing and sharing spatially referenced resources. It enables standardized metadata creation following international specifications such as ISO 19115 and INSPIRE, ensuring data discoverability, interoperability, and long-term accessibility. All metadata records are freely accessible through the IADC catalog at https://metadata.iadc.cnr.it (see supplementary material, last access 10/11/2025).

https://doi.org/10.5194/essd-2026-501
Preprint. Discussion started: 22 July 2026

The research data are distributed through ERDDAP, an open-source data server, developed by NOAA, that provides a consistent interface for searching, visualizing, and downloading environmental data in various common formats (e.g., CSV, NetCDF). ERDDAP simplifies access to time-series and multidimensional datasets, supporting interoperability and facilitating data reuse by the scientific community. The IADC ERDDAP server is available at https://data.iadc.cnr.it.

Through the GeoNetwork interface, it is also possible to request the assignment of a Digital Object Identifier (DOI) for datasets, thanks to the association of the National Research Council of Italy with DataCite. This service enhances data traceability, citation, and long-term preservation in accordance with international data management best practices. In the IADC metadata portal, the metadata structure has been updated to ensure full compliance with the DataCite metadata schema as defined by the DataCite Metadata Working Group (2024), to maximize the discoverability, citation, and linkage of their metadata to the original research. The data published in IADC are federated with the marine data portal IT-IOOS developed in the context of the ITINERIS project (Nestola et al., 2025) and SIOS. Metadata and data management systems have been designed and implemented in alignment with the FAIR principles — ensuring that data are Findable, Accessible, Interoperable, and Reusable (Wilkinson et al., 2016, Tanhua et al., 2019). Each dataset part of this work has a DOI and the full list with metadata landing pages, ERDAPP and DOI is available in the Annex I. This approach promotes transparency, enhances scientific collaboration, and maximizes the long-term value of research outputs produced by the Italian Arctic scientific community.

7 Results

7.1 Hydrodynamic records

Hydrodynamic measurements on the coastal mooring sites (MDI, MAP, and KIM) reveal distinct current patterns shaped by local coastal morphology and site-specific exposure. Below, we present the main characteristics of the current field and its seasonal climatology.

At the MDI site in inner Kongsfjorden, measurements from 2021–2025 show that current directions display a clear bimodal distribution aligned with the fjord axis (~120° and 300°N) (Figure 2a). Currents are generally weak (mean: 0.024 ± 0.022 m s^{-1}), and no consistent vertical pattern emerges along the water column, although a weak tendency toward inflow in the upper layers and outflow in the intermediate and bottom layers is observed (Figure 2a). The time-series indicates that accelerations in the flow occur during episodic events, primarily affecting the uppermost and deepest layers, and there are periods when the flow direction is nearly uniform (i.e., barotropic conditions) throughout the entire water column (Figure 2b). Each year, typically between February and April, a gap in the upper-layer data appears due to poor signal quality. During winter, sea-ice formation leads to exceptionally calm surface conditions and a marked reduction of scatterers in the water, which degrades the ADCP signal and results in data loss near the surface and occasionally throughout the full depth range (Ho Kyung Ha et al., 2015; Kanarik H. et al., 2025). Currents remain persistently weak, and even episodic current pulses rarely exceed 0.1 m s^{-1}. Monthly mean current speed calculated over the full time series (Figure 2d) show an annual cycle characterised by weak

https://doi.org/10.5194/essd-2026-501
Preprint. Discussion started: 22 July 2026

Open Access Earth System Science Data Discussions

variability, but the range of variability is slightly greater between July and February and reduced between April and June (see standard deviation vertical bars of Figure 2d).

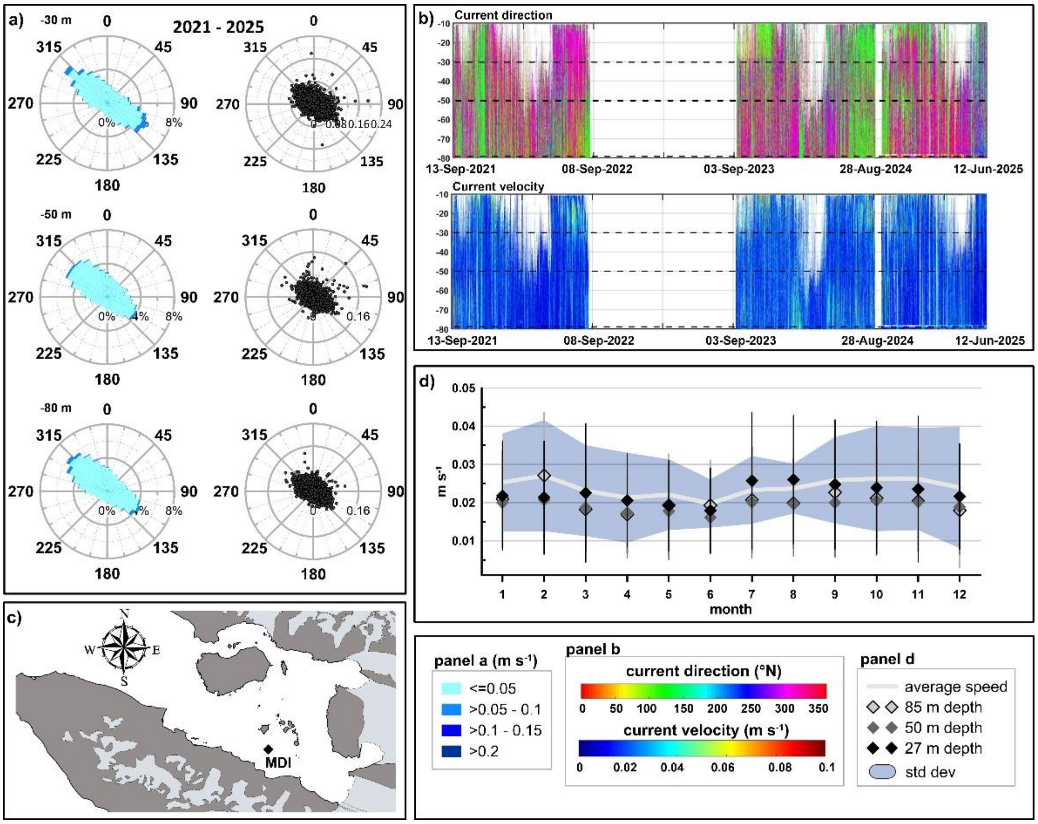

Figure 2: Hydrodynamic records from ADCP at MDI mooring site; a) polar histogram at left and polar scatter at right of speed/direction of currents at three depth layers (30, 50, 80m); b) speed and direction of current along the sounded water column; c) map of mooring MDI location in Kongsfjorden; d) monthly mean of current velocity calculated at three depth layers and averaging the total water column.

At the MAP site, located in the mid-fjord region, hydrodynamic conditions during 2020–2025 are strongly influenced by local morphology, particularly the Brandal Pit, which channels the dominant outflow northward (345°–30°N) and reflects a marked alongshore littoral drift (Figure 3a). Mean current speed is 0.04 ± 0.03 m/s, with maximum recorded velocities reaching 0.41 m s^{-1} during the 23/01/2024. Southward-directed currents are uncommon, occurring with frequencies less than 4% throughout the year, considering the 5° interval histogram bar of Figure 3a. The time-series (Figure 3b) reveals annual recurrence of flow acceleration, concentrated between September and March with the most intense events occurring predominantly in winter, as also indicated by the monthly mean (black line in Figure 3d) that highlight the year-around evolution of the current field (Figure 3d) with general intensification during winter months and weakening between June and July.

https://doi.org/10.5194/essd-2026-501
Preprint. Discussion started: 22 July 2026

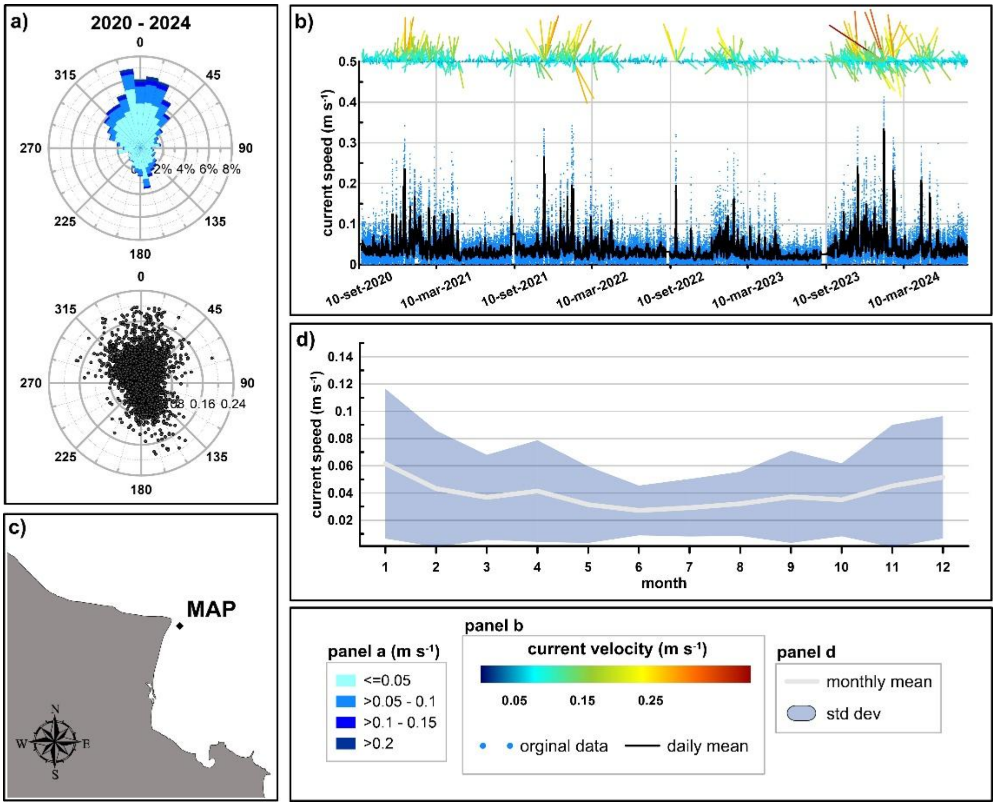

Figure 3: Hydrodynamic records from DCS at MAP mooring site; a) polar histogram and polar scatter of speed/direction of currents; b) current speed (black line is daily smooth while dots are original records) and related vector plot indicating the direction of the currents; c) map of mooring MAP location in Kongsfjorden; d) monthly mean of current speed.

At KIM, in the Krossfjorden, current measurements (2023–2024) collected in the deep layer between 319 and 111 m depth, reveal a bimodal distribution aligned with the fjord's north–south orientation (210°-30°N), with the pattern becoming more pronounced toward the bottom. Strong vertical variability is evident throughout the water column in both flow direction and magnitude. The upper layer (~150 m) is dominated by prevailing inward flow (315°–0°N), whereas at intermediate and deeper levels (approximately 240-300 m) southward-directed currents (165°–180°N) occur more frequently (Figure 4a). These events are particularly pronounced at intermediate depth (240 m) where they are more frequent and current velocity can exceed 0.1 m s^{-1}. The dominant northward flows exhibit a slightly eastward rotation with increasing depth (345°–15°N). Mean current speed is 0.04 ± 0.002 m s^{-1}, with maximum velocities reaching 0.67 m s^{-1} during the 02/11/2023. The time-series (Figure 4b) shows that enhanced hydrodynamic activity is concentrated between 150 and 250 m depth, while below this water layer the currents are generally weak-except during winter 2024, when strong pulses appear near the seabed. During this period (March - April) much of the water column is disturbed, resulting in reduced data quality. Flow rotation is not associated with the occurrence of current pulses, which are observed during both inflow and outflow. The monthly mean pattern (Figure 4c)

https://doi.org/10.5194/essd-2026-501
Preprint. Discussion started: 22 July 2026

Open Access Earth System Science Data Discussions

indicates a clear annual cycle, characterised by pronounced vertical variability between 150 and 300 m depth and greater hydrodynamic activity in winter and spring, followed by marked weakening currents during summer (June - September).

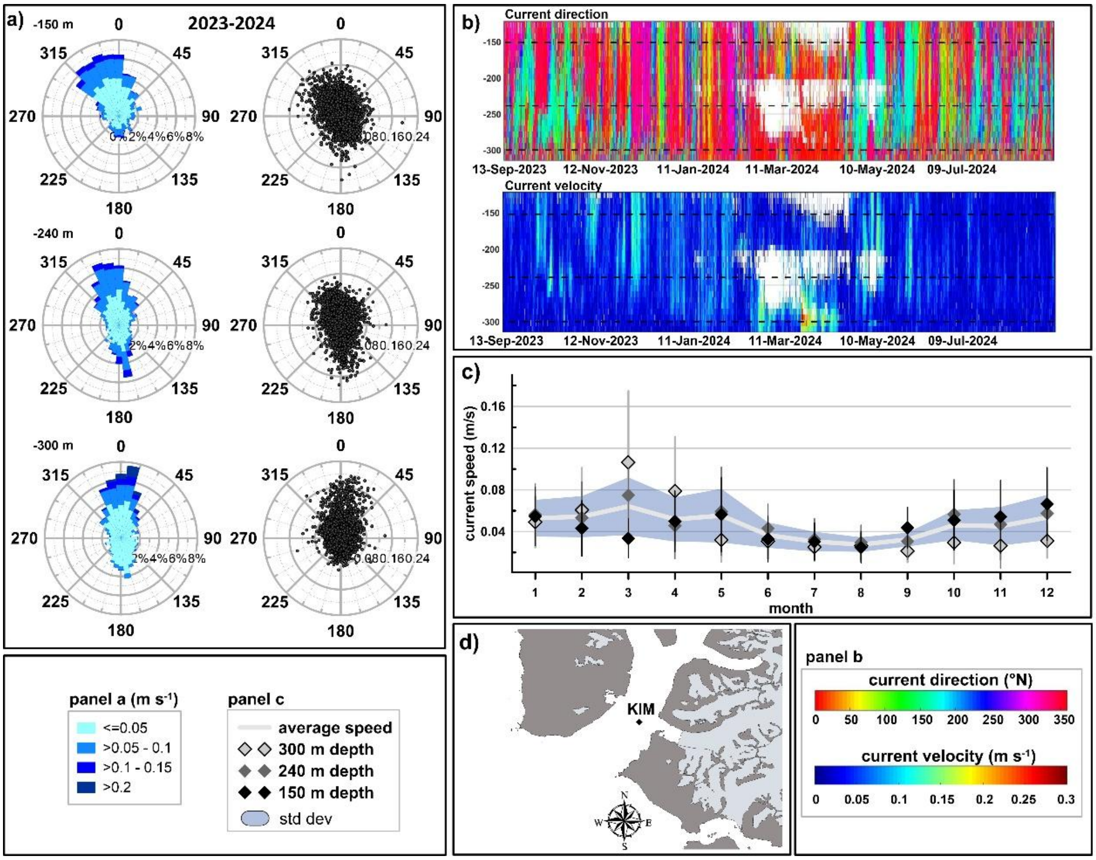

Figure 4. Hydrodynamic records from ADCP at KIM mooring site; a) polar histogram at left and polar scatter at right of speed/direction of currents at three depth layers (151, 240, 303m); b) speed and direction of current along the sounded water column; c) monthly mean of current speed calculated at three depth layers and averaging the total water column; d) map of mooring location in Krossfjorden.

At the offshore S1 mooring site, the current field is characterised by two dominant directional sectors (Figure 5a) oriented in opposite directions along the SE–NW axis. This bidirectional pattern is most prominent between 1000 and 800 m depth. Above this layer, the flow becomes more coherent, with a prevailing north-westerly direction (Figure 5a). Between 2020 and 2023, the current regime exhibits quite cyclical intensification during the autumn period (Figure 5b) but a marked strengthening of the current field is also observed in spring 2022, when the strongest currents are directed toward the SE. Reversals of current direction toward south-east are episodic and more frequent during the autumn-winter period between 750 and 1000m depth whereas above these depths such reversals are markedly less frequent. These observations indicate that no specific period is uniquely associated with the episodes of the current intensification and reversal. Throughout the water column, the

https://doi.org/10.5194/essd-2026-501
Preprint. Discussion started: 22 July 2026

hydrodynamic structure remains relatively uniform, with no pronounced vertical gradients in current intensity (Figure 5b and c). Mean current speeds range from 0.15 to 0.12 m s^{-1} between 550m and 1000 m depth, with standard deviations between 0.07 and 0.09 m s^{-1}. Average velocities reach their maximum at 1000m depth and their minimum at 700m depth. Maximum current intensities display a similar vertical pattern, decreasing from 0.60 m s^{-1} at 1000 m to 0.43 m s^{-1} at 700 m. The year-around pattern of current intensity (Figure 5d) reveals limited variability both vertically and seasonally, with a general weakening of currents in September and enhanced variability primarily between January and May.

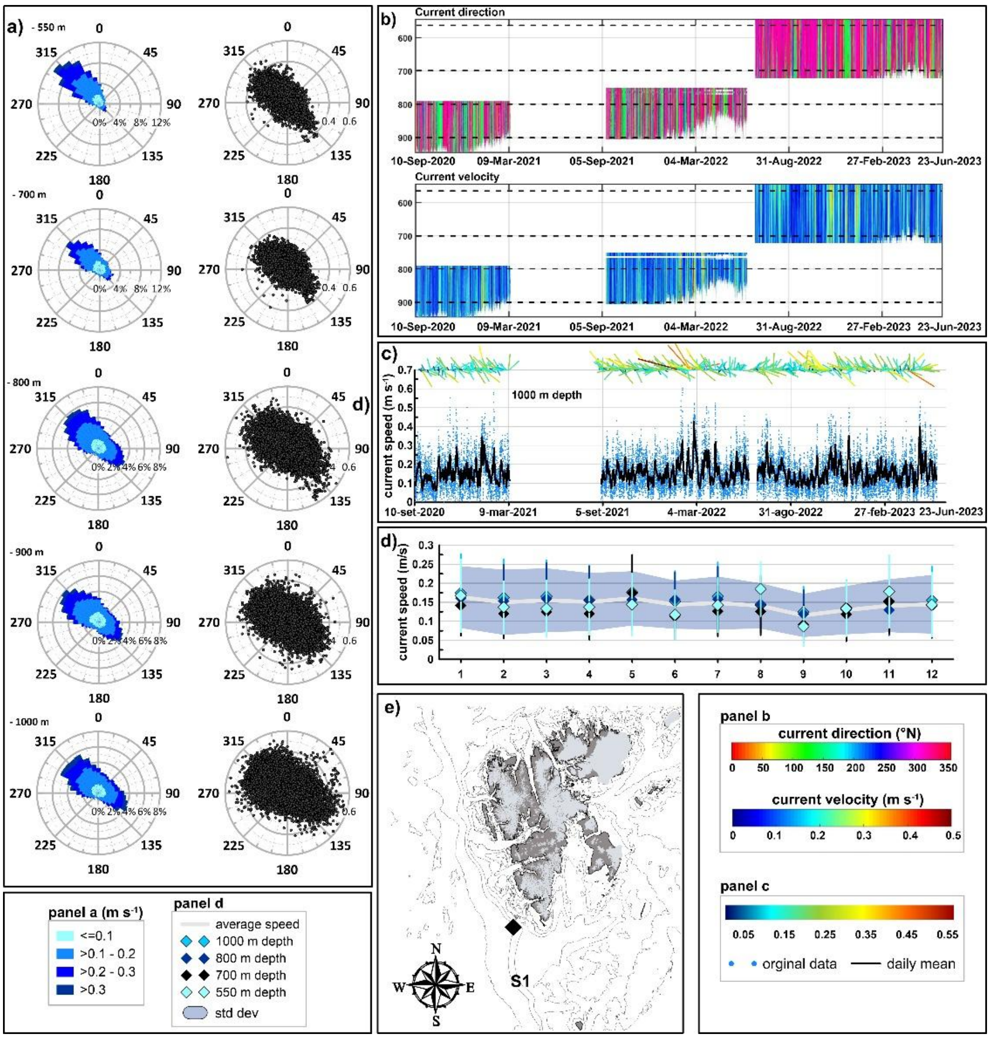

Figure 5. Hydrodynamic records from ADCP at S1 mooring site; a) polar histogram (left) and polar scatter (right) of speed/direction of the currents recorded by ADCP between 2020 and 2023 at four depths (550, 700, 800, 900, 1000m) and between 2020 and 2023 at 1000m by DCS; b) velocity and direction of currents recorded along the sounded water column; c) time-series of current and direction of velocity measured by DCS at 1000m depth; d) monthly mean of current speed calculated at four depth layers and averaging the total water column; e) map of mooring location in the Fram Strait south of Spitsbergen

https://doi.org/10.5194/essd-2026-501
Preprint. Discussion started: 22 July 2026

7.1.2 Seasonality of currents and relations among sites

The variability of hydrological conditions in the different mooring sites is observed at seasonal scale and discussed in relation to the wind variability, observing general linkage between hydrodynamics and wind patterns. Wind data were obtained from the anemometer mounted on the CCT station at Ny-Ålesund and from the Kvadehuken anemometer operated by the Norwegian Centre for Climate Services (NCCS), both installed at a height of 5m height (Figure 1b, red triangles). These two anemometers were selected because of their complementary positions: the CCT station located inside the fjord, and the NCCS station positioned at the exposed southern tip of the Kongsfjorden headland. Seasonal variability in current speed at MDI and KIM was assessed at three levels throughout the water column (depth levels indicated in Figures 2 and 4 with dotted lines) while at S1 depth levels every 100-150 m are selected (depth levels indicated in Figures 5 with dotted lines).

The well-apparent seasonal variability of the currents at all the three sites within the Krossfjord-Kongsfjord system (Figure 6 c,d,e) is analysed with respect to the seasonal wind patterns (Figure 6 a,b). Data winds recorded at the CCT (Figure 6a) show a prevailing South-East direction, with a secondary sector from the South-West more frequent and intense in Summer. In Spring and Summer, the frequency of events originating from the North-West increases, although it never exceeds 8% for each histogram bar spaced every 5°. At the tip of the promontory (Figure 6b), where the Kvadehuken NCCS station is located, the wind regime displays a trimodal pattern of wind provenance influenced by seasonal variability. During Autumn and Winter, winds primarily come from the East - South-East, whereas in Spring the winds arrive with similar frequency from South, North and East - Southeast. In Summer, winds from the South become more pronounced.

https://doi.org/10.5194/essd-2026-501
Preprint. Discussion started: 22 July 2026

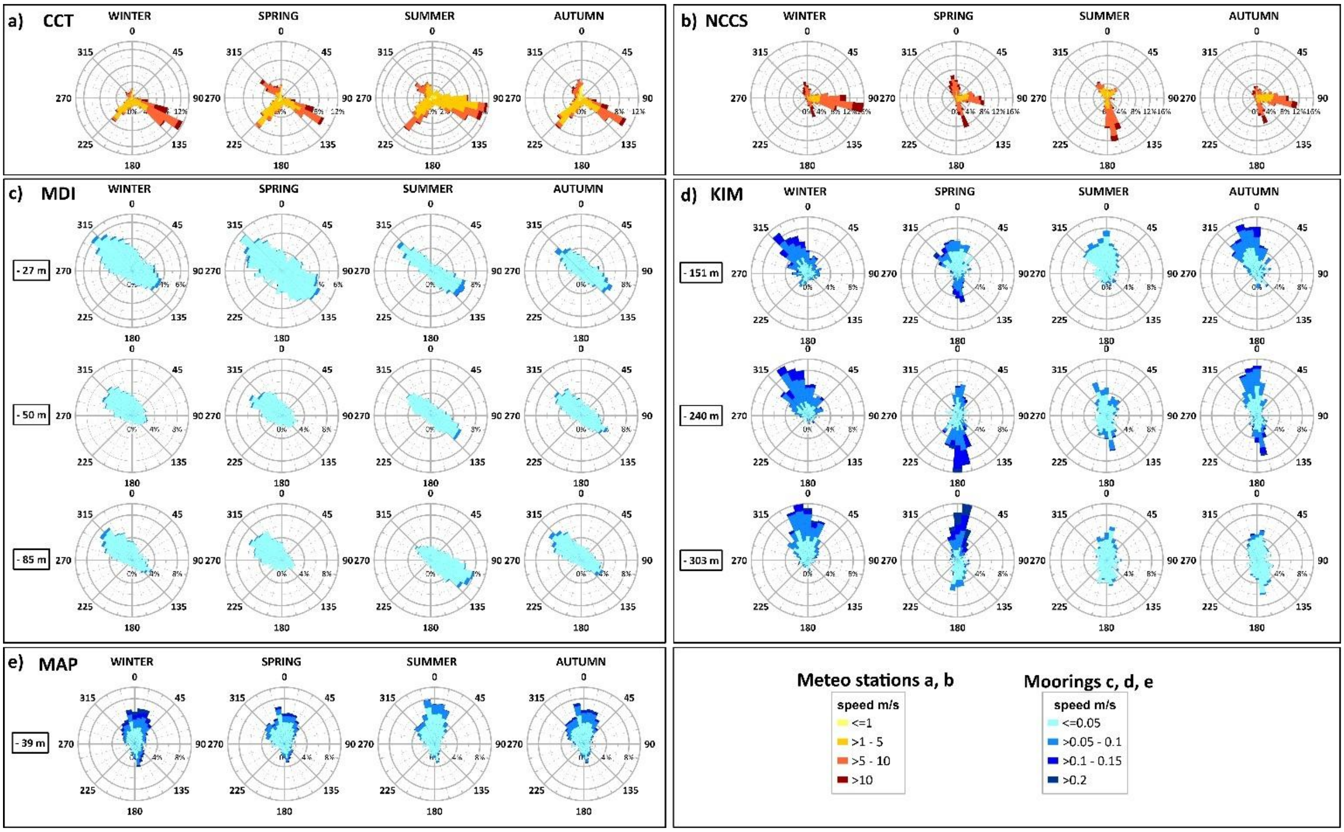

Figure 6. Seasonal variability of the currents and wind in the Krossfjorden-Kongsfjorden system; a) seasonal wind histogram polar plot from CCT station; b) seasonal wind histogram polar plot from NCCS station; c) seasonal current histogram polar plot from MDI mooring at three depth levels; d) seasonal current histogram polar plot from KIM mooring at three depth levels; e) seasonal current histogram polar plot from single depth measurement on MAP mooring.

Currents at MDI maintained a bimodal pattern with two main directions (~120° and 300°N) aligned with fjord axis orientation during all seasons. The seasonal variability is mostly related to the direction of the flow despite intensity, which remains always weak and very similar with average values of 0.022 ± 0.023 m s^{-1} during Winter and 0.019 ± 0.017 m s^{-1} during Spring. In the upper layer (27m depth) during winter and spring the currents are distributed over a wide range of directions while during summer autumn the directional spreading is in a narrower range. The southwestern component observed in the polar wind histogram is not represented in the hydrodynamic field where the two aligned-fjord axis directions dominate. During Winter winds intensify and are mainly from South while ocean currents at MDI show dominant direction toward North-West (315°) outflowing the fjord especially at 50 and 85 m depth. In Spring the component from North-West of wind increase and show a prevailing moderate intensities (> 5 m s^{-1}). Currents at depth show the same pattern observed in Winter while at 27 m the inflow and outflow directions are balanced. During Summer, prevailing winds rotate to the East (100°N), southwestern component increases, and north-western component decreases in terms of average intensity; the prevailing directions of currents especially at 50 and 85 m depth rotate in the opposite directions to 120°N. The dominant wind rotates again from

https://doi.org/10.5194/essd-2026-501
Preprint. Discussion started: 22 July 2026

Open Access Earth System Science Data Discussions

South-East and increases the component of wind from North during Autumn. The hydrodynamic field at 27 and 50m is characterised by a balanced frequencies of inflow and outflow directions while at 85m the prevailing directions of currents are north-westward.

At MAP directional distribution remains consistent across seasons, though intensity peaks in winter (average 0.05 ± 0.04 m s^{-1}) and weakens in summer (average 0.02 ± 0.02 m s^{-1}). Maximum value recorded during different seasons show a seasonal fluctuation with maximum current intensity during winter (0.41 m s^{-1}) while in summer maximum speed reaches 0.17 m s^{-1}. The southward directed currents have similar frequencies during different seasons but are more intense during Winter (0.041 ± 0.038 m s^{-1}), reaching a maximum intensity of 0.32 m s^{-1}. The seasonal variations in the wind field do not reflect any changes in the directional distribution of currents which remain strongly aligned with the coastal and bottom morphology.

At KIM the variability of currents is marked, both seasonally and vertically. During Winter, the wind field is characterised by a dominant direction from East (100°N) and two less frequent opposite components (< 10%) South-East - North-West (160° - 350°). The currents during Winter feature dominant inward flow, rotating to North (350°N) moving downward with an average intensity of 0.05 ± 0.03 m s^{-1}. The component from North - North-West exceed frequently 0.1 m s^{-1}. During Spring, the wind from East drastically reduces and the component from North-West (350°N) increases together with the opposite wind from South-East (160°N). The flow at 150m is bidirectional with wide directional spreading of the inflow current toward north while southward currents are limited in a narrower range. Moving deeper there are two layers with opposite directions with a dominant southward flow (165°–180°N) at 240m and northward (0°–15°N) at 300 m that in both cases can exceed 0.2 m s^{-1}. During summer the prevailing direction of wind is from South (160°N) and the other two components (East and North) reduce both their frequencies and intensities. Summer currents weaken significantly (0.03 ± 0.02 m s^{-1}) and maximum velocities do not exceed 0.2 m s^{-1}; the flow at 150m moving mainly northward while going deeper the frequency of inflow and outflow directions are more balanced. In autumn the wind field is mainly characterised by the increase of easterly wind and great reduction of northerly component. The currents intensify again with notable frequencies of events above 0.2 m s^{-1}, showing a variable hydrodynamic pattern with northward inflow dominant at 150m and balanced outflow-inflow currents at 240 and 300m depth reducing their intensity with depth.

https://doi.org/10.5194/essd-2026-501
Preprint. Discussion started: 22 July 2026

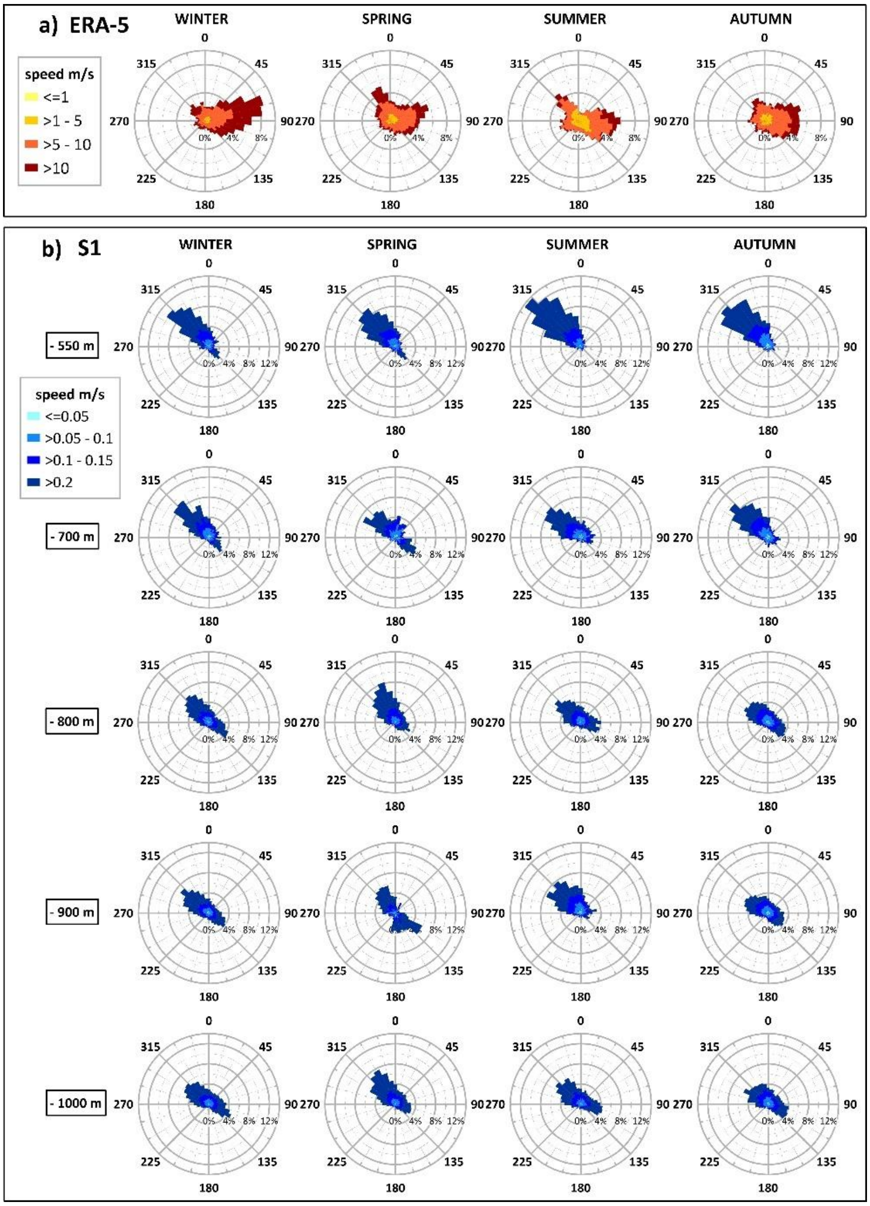

Figure 7. Seasonal variability of the currents and wind in the site of S1 mooring in the Fram Strait; a) seasonal wind histogram polar plot from ERA-5 meteorological data; b) seasonal current histogram polar plot from S1 mooring at five depth levels.

The seasonal and vertical variability of currents at the S1 site, located offshore the South Cape of the Spitsbergen, is evident throughout the water column (Figure 7) and is not directly related to variations observed in the seasonal wind patterns (Figure 7a). Wind data from the ERA5 ECMWF global reanalysis indicate a prevailing easterly and north-easterly wind across all seasons with intensity decreasing from Winter to Summer. The main seasonal shift is related to the increase of a secondary north-westerly component during Spring and Summer. During Spring, this component slightly rotates to northern directions (330-340°N), whereas in summer it rotates to 315-330°N, accompanied by a small component of low frequent westerly winds.

https://doi.org/10.5194/essd-2026-501
Preprint. Discussion started: 22 July 2026

At 550m the currents (Figure 7b) are primarily directed north-westward, and this direction dominates across all seasons; however, during Winter and Spring, a minor south-eastward component is also observed. The intensity of currents varies vertically and during seasons at 550m and the average intensity ranges between 0.13 and 0.15 m s^{-1} with maximum values observed in spring (0.52 m s^{-1}). At 700 - 900 m average current speed during the different seasons is quite similar (0.12 - 0.13 m s^{-1}) but the largest velocities are observed in Spring (0.47 m s^{-1}). Near the bottom (1000 m), the average intensity across the seasons varies between 0.14 and 0.16 m s^{-1} and the largest velocity was observed during the Autumn with very strong currents that reach 0.8 m s^{-1} but also in the other seasons at this depth the maximum intensities are between 0.47 and 0.55 m s^{-1}. Starting from 800m depth the southern component is visible also in Autumn while sensitively decreases moving upward with a main flow directed toward North-West. Going deeper, this secondary component becomes more frequent, and in the deepest layer it is consistently present throughout the year and collectively account for the 38 and 39% of the total events at 800 m and 1000m while seasonally the currents toward south have the maximum frequency during Winter and Autumn with a both similar frequency of approximately 30% of the total southward events. The dominant northward flow rotates slightly toward North during Spring starting from 800m depth while in Summer at all depths the flow rotates slightly westward.

7.2 Thermohaline records

7.2.1 Regional climatology and vertical structure

Thermohaline records from all moorings exhibit ranges of variability determined by the seasonality whose amplitudes vary also with depth and distance from shore (Table 2). At the moorings located into the fjords (MDI, MAP, KIM; −22 to −120 m), Conservative Temperatures (CT) ranges from winter minima of ~−1.8 to −0.9 °C, to summer maxima of 6.3–8.9 °C. Mean CTs spans 1.9–2.7 °C, with the greatest variability at the shallowest sensors (standard deviation up to ±2.5 °C). In contrast, the deep offshore site S1 (−820 to −1000 m) shows reduced thermal variability, with mean CT near 0 °C and a narrow range of variability (−1.02 to 3.77 °C), consistent with weak variability in deep waters. Absolute Salinities (SA) at coastal moorings follow a seasonal cycle with an opposite behaviour with respect to temperature (higher salinity in the cold season, lower in the warm season). Mean SA lies between 34.57 and 34.93 g kg^{-1}, with variability up to ±0.44 g kg^{-1} at the most surface influenced sensor and a wide overall range (32.08–35.14 g kg^{-1}), because of exposed to freshwater and Atlantic water masses influence. At S1, salinity is highly stable (mean 35.07–35.09 g kg^{-1}; variability ≤ ±0.01 g kg^{-1}; range 35.01–35.18 g kg^{-1}), reflecting well stratified deep-water masses.

Mooring	Depth	Mean CT ± SD (°C)	Min - Max CT (°C)	Mean S_A ± SD (g/kg)	Min - Max S_A (g/kg)
MDI	-27 m	2.14 ± 2.51	-1.79 - 8.74	34.56 ± 0.43	32.08 - 35.14

https://doi.org/10.5194/essd-2026-501
Preprint. Discussion started: 22 July 2026

	-89m	1.91 ± 2.10	-1.78 - 6.83	34.85 ± 0.12	34.16 - 35.20
MAP	-20m	2.44 ± 2.51	-1.752 - 8.87	34.59 ± 0.35	32.31-35.12
	-39m	2.34 ± 2.17	-1.718 - 7.83	34.68 ± 0.30	33.09 - 35.13
KIM	-65 m	2.70 ± 2.23	-0.855 - 8.26	34.80 ± 0.20	33.72 - 35.16
	-120m	2.29 ± 1.72	-0.933 - 6.37	34.92 ± 0.11	34.36 - 35.31
S1	- 820	0.062 ± 0.67	-0.80 - 3.77	35.08 ± 0.010	34.94 - 35.17
	-940	-0.496 ± 0.41	-0.88 - 3.56	35.07 ± 0.005	35.008 - 35.16
	-1000	-0.758 ± 0.17	-1.02 - 2.91	35.07 ± 0.002	35.03 - 35.15

Table 2: Statistical parameters of Temperature and Salinity measured at level depth on different mooring sites

The thermohaline structure of the water column observed since 2020, based on multiple evidence from sensors installed along the water column, exhibits a clear annual cycle with summer warming and winter cooling modulated by site-specific stratification. The interpolation of temperature values recorded along the water column (Howmoller diagrams in Figure 8) at coastal mooring sites are consistent with an annual cycle characterised by different phases of water column stratification. The vertical evolution of temperature (Figure 8) together with salinity records highlight site specific features:

- MDI: Upper layer warming above 50 m begins in spring and peaks in summer usually at the end of August and in 2023 the warming of the upper layers (27m) is particularly pronounced respect the deeper and reaches 8.7°C. At the end of October, the upper layers start cooling while deeper (90 - 95m) show higher temperature until the end of November when all water columns have a small positive drop with temperature around 4.5 - 5°C. Thermal variability is accompanied by salinity variations strongly pronounced on the upper depth level where the salinity variations occur between June and December. This behaviour is less pronounced at depth (90 m) where weak variations and evident stratification occur during this period while between January and May the water column be clearly mixed.
- MAP: Thermal variations in this shallow site have a limited vertical gradient (~1 °C) between 20–40 m. During summer 2023 severe warming of the upper layer occurs exceeding 8 °C. Despite the limited thermal variability salinity variations are more pronounced especially during summer-autumn 2024, with pronounced stratification between 20 and 35 m depth.
- KIM: The seasonality is evident but less marked especially for salinity due to higher depth, position far from freshwater source and near the fjord entrance. Summer warming initiates near the surface from June and the warm core subsequently migrates downward to ~150–200 m from late summer to autumn, while the surface layer cools. Stratification is particularly evident between June and the end of December and at 300 m depth warming is less evident and does not exceed 3°C. Between January and June the water column is mixed and reaches values below 0°C during March and April. Salinity is less variable between the two depth levels (-65, -120m) but more marked on the upper level but not exceeding 1 g Kg-1. The

https://doi.org/10.5194/essd-2026-501
Preprint. Discussion started: 22 July 2026

Open Access Earth System Science Data Discussions

freshening is evident between September and December at 65 m depth while homogeneous values can be observed from January to June.

- S1: Temperature decreases with depth from ~795 to 1020 m, but episodic intrusions of warmer water (T > −0.5 °C) reach the deepest levels especially during Winter. Similarly, salinity decreases moving downward along the water column and the episodic increases coincide those observed in temperature and involve the whole observed water column.

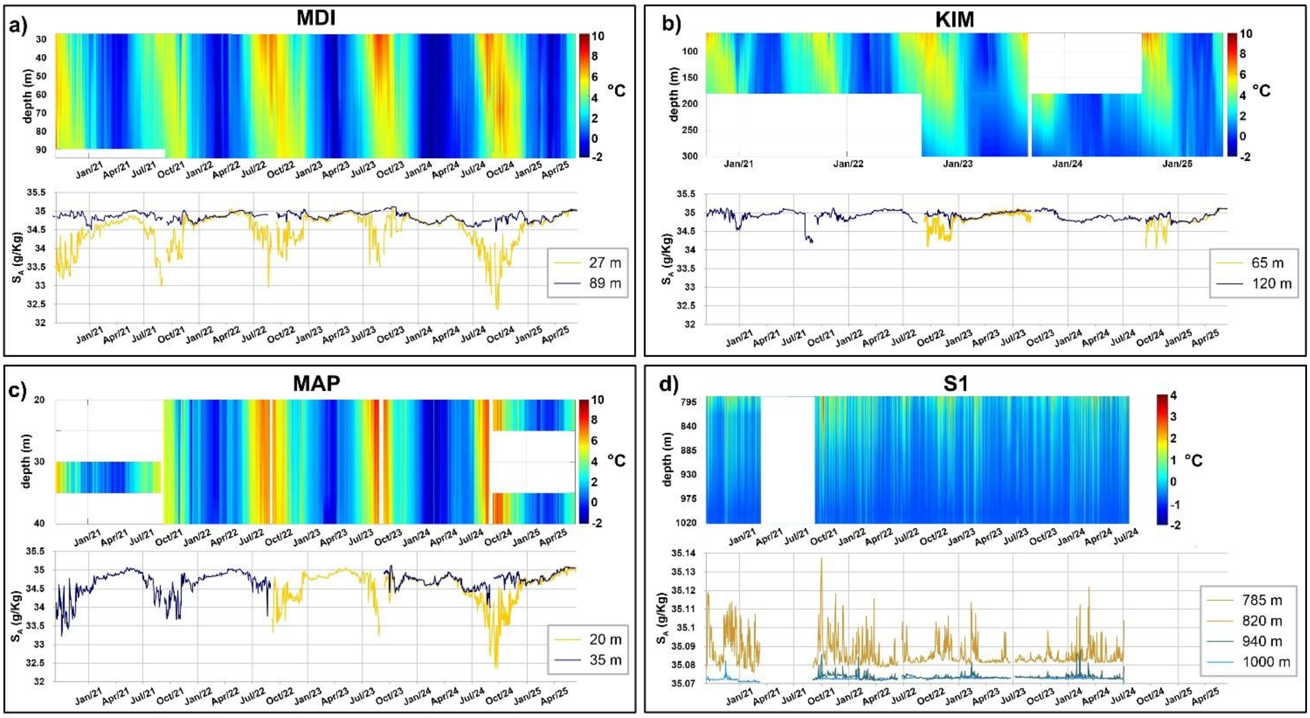

Figure 8. Time series of conservative temperature and absolute salinity recorded during 2020 – 2025 at mooring locations along the water column. For each panel a) MDI, b) KIM, c) MAP and d) S1 there is the Howmoller diagram that merges all temperature measurements (see Table 1 for depth levels), and Absolute Salinity (SA) time series at discrete depth levels.

Monthly means (solid lines) and standard deviations (shading) show the annual climatology at the CTD levels per each mooring (Figure 9: CT maxima occur in August at MDI and MAP, and in September at KIM). At MDI, warming at 27m leads the deeper layer (89m) by ~2 months, while at KIM, warming at 65m depth leads the deeper layer (120 m) by ~1 month. At MAP, the behaviour of the two depth levels at 22 and 39m are synchronous but more pronounced in the upper layer. In detail, MDI at 27 m during August shows a peak mean temperature of 6.67 °C (max 8.74 °C), while at 89 m in October, the peak mean temperature is 5.03 °C (max 6.83 °C). KIM at 65 m in September show a peak mean temperature of 6.25 °C (max 8.26 °C), while in in October at 120m the peak mean temperature is 4.72 °C (max 6.37 °C). Winter minima are observed in the upper levels at MDI and MAP in February and March (MAP −1.75 to −1.67 °C; MDI −1.79 to −1.78 °C); at KIM minima occur at 120 m (−0.93 to −0.90 °C). The seasonal structure of salinity at deeper levels of MDI (89 m) and KIM (120 m) show a bimodal cycle with peaks in May (means 34.94 and 35.01 g kg^{-1}; maxima 35.20 and 35.24 g kg^{-1}) and October (means 34.89 and

https://doi.org/10.5194/essd-2026-501
Preprint. Discussion started: 22 July 2026

34.98 g kg⁻¹; maxima 35.13 and 35.23 g kg⁻¹). MAP lacks the autumn peak and becomes more variable from July onward. Pronounced upper layer freshening starts in June at MDI (27 m) and MAP (20 m) and is weaker and delayed to July at KIM (65 m); the summer autumn minima reach 32.08, 33.72, and 33.09 g kg⁻¹ at MDI, KIM, and MAP, respectively. KIM exhibits the smallest annual variability in both CT and SA, as indicated by the narrowest standard deviation bands throughout the year.

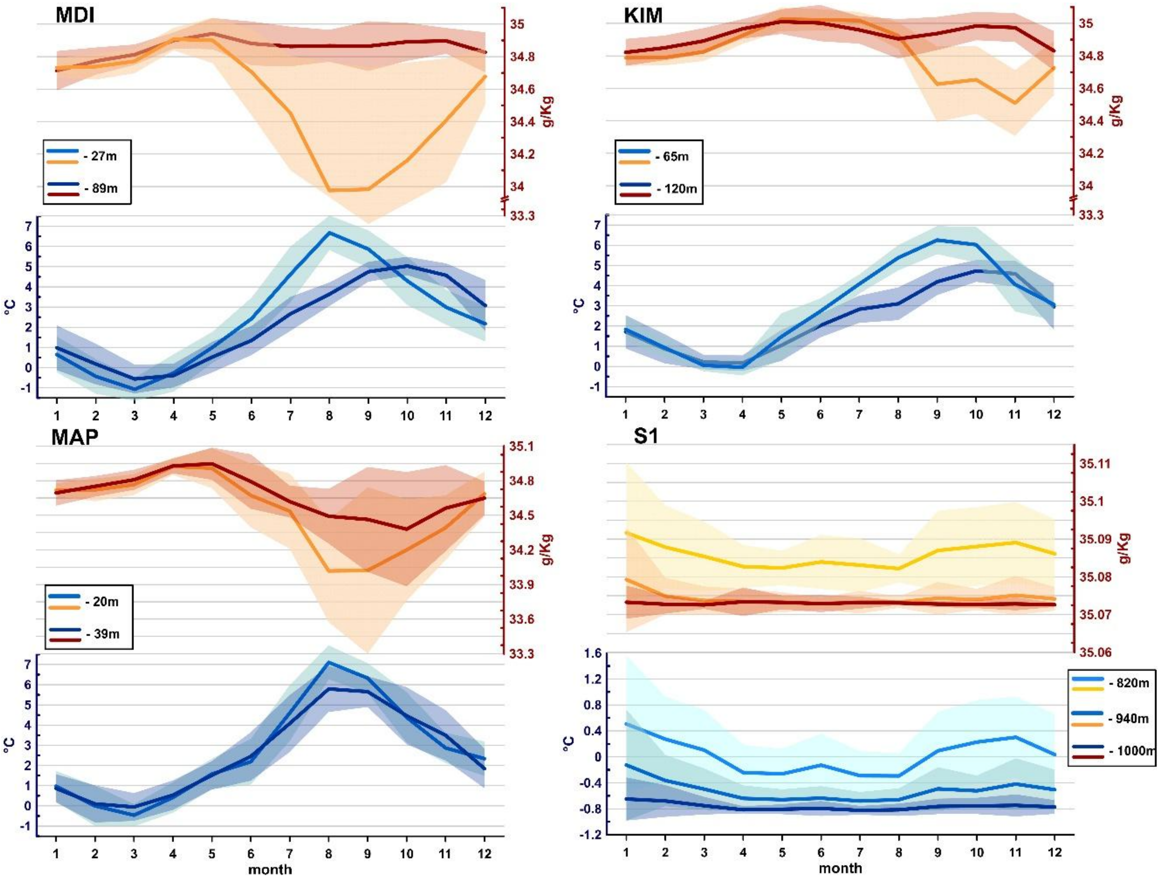

Figure 9. Monthly mean of Conservative Temperature (CT) and Absolute Salinity (S_A)computed along the water column in the different mooring sites.

Thermohaline conditions measured at the deepest level of each mooring site are used to define water masses grouped at monthly scale. Water masses are categorised starting from CT and S_A values following the classification proposed by Tverberg et al. (2019), Skogseth et al. (2020) and De Rovere et al. (2020). At S1, AW are identified using temperature threshold ≥ -0.5°C (Bensi et al., 2025). This criterion is applied in comparison to the occurrence of Eurasian Basin Deep Water, called Norwegian Deep Sea Water (NSDW), which typically characterises the deepest water layer with temperature < -0.6°C, and salinity > 34.9 (i.e., 34.915 for this specific definition from Rudels, 2009). In Figure 10, each panel corresponds to a mooring site, and the vertical bar plots depict the monthly frequency of water masses interesting the sites.

At MDI (Figure 10a), Transformed Atlantic Water (TAW) and Intermediate Water (IW) represent the prevailing water masses from June to December while from February to May WCW and LW represent a frequency greater than 58%. From March to

https://doi.org/10.5194/essd-2026-501
Preprint. Discussion started: 22 July 2026

May the inner part of Kongsfjorden is interested by the inflow of ArW with a frequency between 20 and 27% while warm and saline AW are observed during September and October 2023 and 2024.

At MAP (Figure 10b), TAW are observed from March to December with larger frequency during May and June (47 - 58%) and IW dominates from July onward while in the first months of the year (January - April) LW have a frequency between 38 and 53%. At this site are also observed SW that recur especially in summer and Autumn with a frequency between 11 and 30%. Cold ArW and WCW are observed during winter and spring months with a frequency around 20%. AW intrusion observed in 2023 are related to events occurred in October.

At KIM (Figure 10c), LW dominates from February to May together with cold ArW (3 - 27%) and TAW is observed all over the year but especially from July until November becomes dominant (44 - 74%) together with IW together accounting for 81-97%. AW are observed from June initially with low frequencies (2-5%) and after with greater frequencies in October and November (14 - 18%).

At S1 (Figure 10d), during spring and summer months (April - August) prevails NSDW while in January and February and in October and November, AW has a frequency between 53 and 63%.

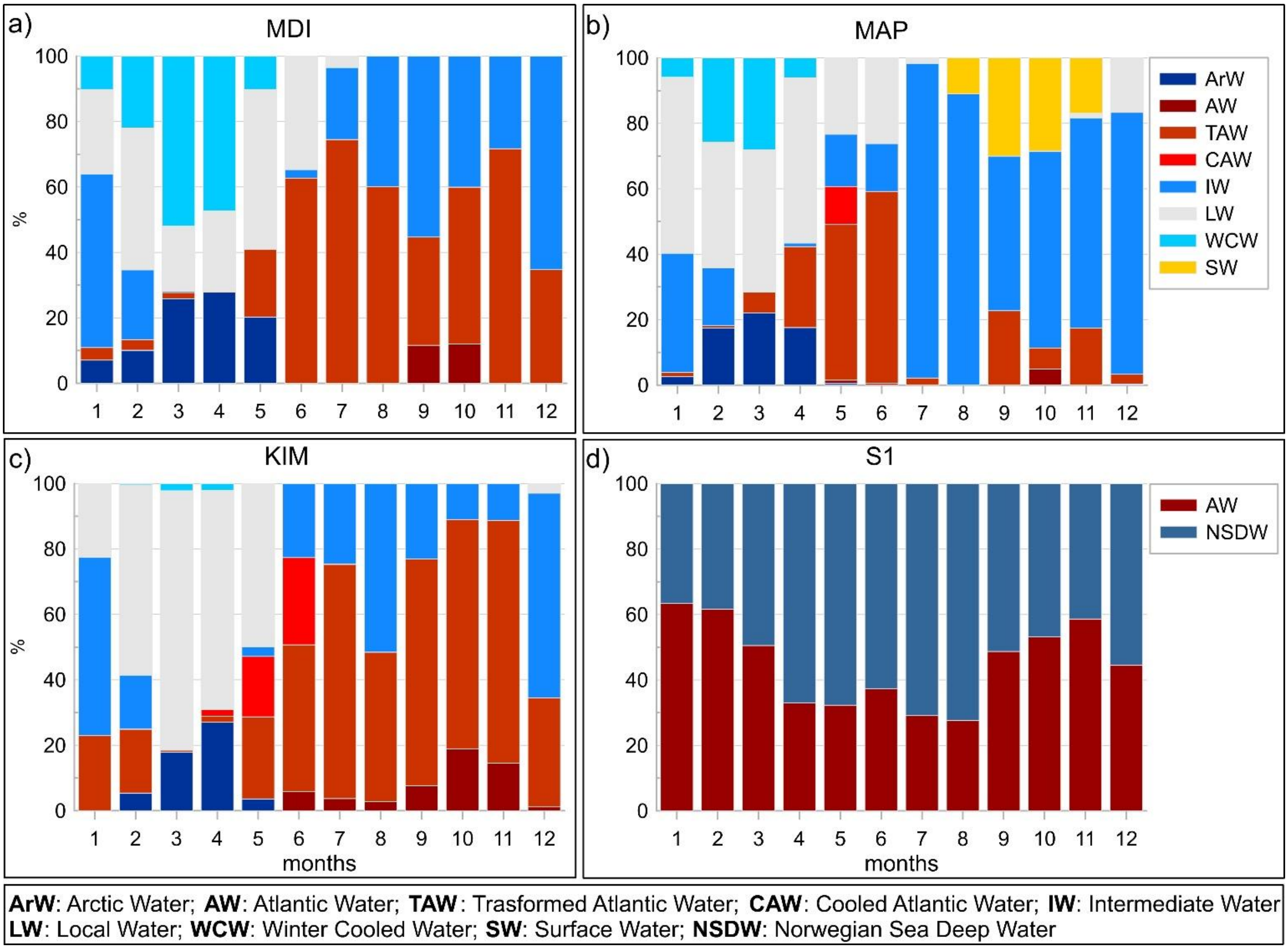

Figure 10. Monthly frequency of water mass type in the different mooring sites; a) MDI; b) MAP; c) KIM; d) S1. The water mass classification (colour coded acronym in the legend) is determined on the deeper sensor of the mooring line. Extended name of each water mass is reported in the bottom panel.

7.2.2 Seasonality and annual variability of water masses

Figures 11–14 present the TS diagrams, illustrating the seasonal evolution of thermohaline properties over the study period, as well as the variability of the mean potential density anomaly and the occurrence frequency of the different water masses at each mooring site.

KIM (Krossfjorden)

- Winter: a pronounced variability is observed in salinity and temperature; IW is the prevailing water masses (>50%) except during 2022 when it is less than 20%. Average density anomaly fluctuates between 27.66 and 27.72 kg m^{-3} and variability of thermohaline properties is particularly pronounced during winter 2022 when warm and saline water masses occur

https://doi.org/10.5194/essd-2026-501
Preprint. Discussion started: 22 July 2026

in the measuring site. Winter 2024 was the year with the largest variability in terms of temperature (range of 5.79°C). Atlantic type waters recur during 2021-2024 with a decreasing trend of frequency with minimum in 2025 (0.49%).

- Spring: variability is reduced, and water masses are particularly dense with average value above 27.8 kg m^{-3} (27.84 - 27.98 kg m^{-3}) and prevailing LW masses; Atlantic type water masses are represented mainly by CAW which show a maximum frequency of 18% in 2024 together with the maximum frequency of ArW (34%). Maximum density was observed during 2022 when cold water masses (ArW, LW and WCW) had the maximum frequency (87%) while the warmest conditions were measured during 2025 (0.79+/-0.91°C).
- Summer: Density anomaly of water masses decreases (27.69-27.83 kg m^{-3}) but remains a restricted variability. The shift is mostly determined by the increase of temperature which shows a range between 1.20 and 4.56 °C; SA varies from 34.71 to 35.16 g kg^{-1}, and the most saline conditions occur in 2023, when also warmest conditions occur (3.07+/-0.88°C). Atlantic type waters dominate this season with frequency larger than 70% except 2024 when IW dominates (88%) and summer 2023 and 2025 are characterised by the inflow of AW. Summer 2025 cannot be completely described because the survey stops in late June, and the frequency are not exhaustive.
- Autumn: we observe the warmest conditions and high variability especially in terms of salinity (CT = 1.91–6.30 °C; SA = 34.64–35.19 g kg^{-1}) and density anomaly varies between 27.5 and 27.66 kg m^{-3}. Dominance of Atlantic water type with TAW always above 56%, and 2021 and 2023 characterised by the presence of AW (11 - 40%). Average temperature is always above 4°C and the warmest autumn was measured in 2022 (5.02+/-0.44°C).
- Seasonal T–S: there is limited spread in spring–summer but during spring densest ArW and LW dominates while in summer and autumn prevails AW and TAW; large fluctuations in autumn–winter, when both T and S variability peak. In winter the lighter IW prevails compared to autumn characterised by more saline TAW and AW masses.

https://doi.org/10.5194/essd-2026-501
Preprint. Discussion started: 22 July 2026

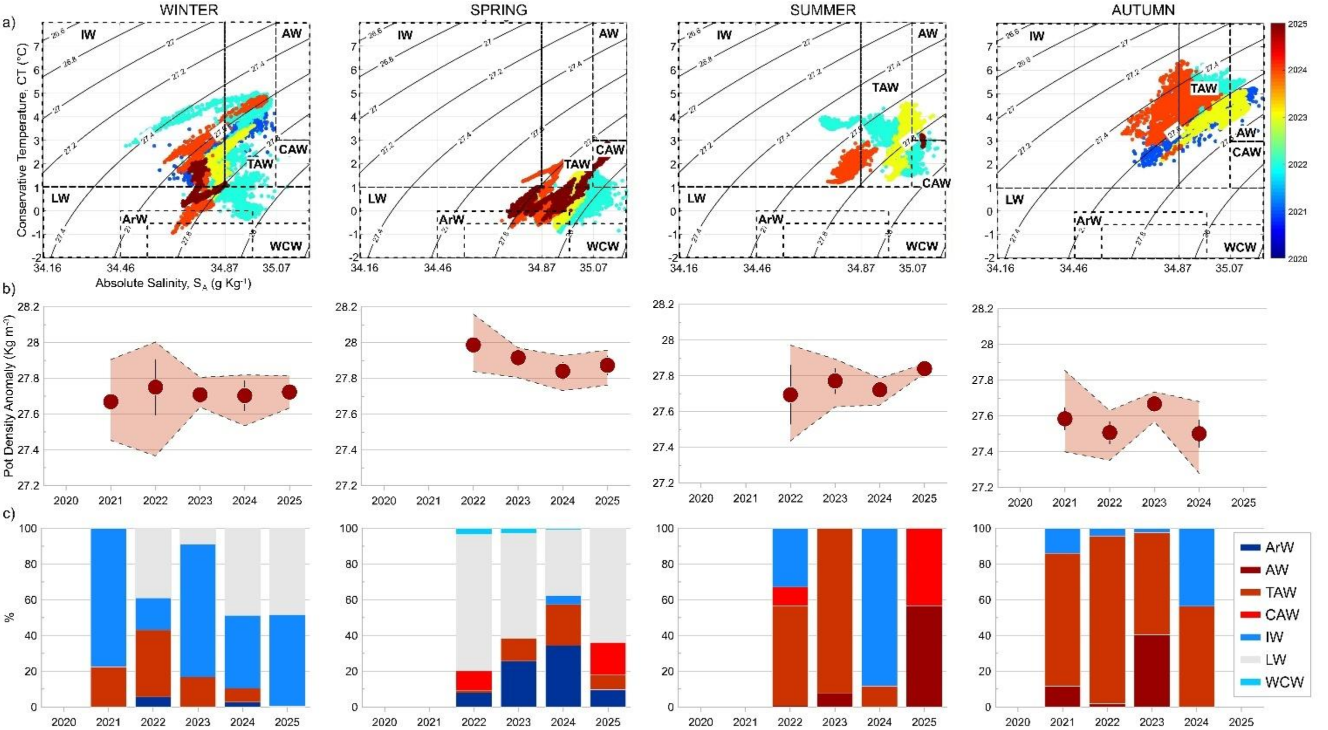

Figure 11. KIM mooring; a) TS diagram during different seasons; color coding represents the different years; b) annual variability of potential density anomaly during different seasons; c) annual variability of water mass frequencies during different seasons. (ArW: Arctic Water; AW: Atlantic Water; TAW: Trasformed Atlantic Water; CAW: Cooled Atlantic Water; IW: Intermediate Water; LW: Local Water; WCW: Winter Cooled Water)

MAP (Kongsfjord, Bayelva river mouth)

- Winter: there is a strong temperature aligned variability and the average density ranges between 27.44 and 27.78 kg m^{-3}. CT between −1.68 and 4.85 °C and SA between 34.20–35.00 g kg^{-1} with prevailing presence of IW and LW that usually account for more than 90% except 2022 and 2024 when occur also ArW and WCW. Atlantic-type waters are rare and occur with very low frequency only in 2022 and 2024 (2.7 - 2.4%).
- Spring: variability is reduced, and water masses are the densest across the seasons; Limited variability is also observed during the years with average density anomaly between 27.77 and 27.87 kg m^{-3}. Observed CT is between −1.71 and 3.14 °C and SA between 34.45 and 35.09 g kg^{-1} with main water masses represented by LW (37 – 76%). The cumulative frequency of Atlantic type waters (TAW and CAW) increases from 11% in 2022 to 26% in 2025. Cold waters (ArW, WCW) prevail in 2024 with a frequency of 48%.
- Summer: there is a broad variability in both temperature and salinity (CT = 0.67–7.83 °C; SA = 33.39–35.07 g kg^{-1}), with the dominant axis of variability being temperature in 2024 and salinity in 2021. Large variability is clearly visible also on the density anomaly which shows a great variability (range of 1.36 - 1.38 kg m^{-3}) every year while the annual mean varies between 27.26 and 27.78 kg m^{-3}. Prevailing water masses are IW but Atlantic type waters occurring during 2021, 2022 and

https://doi.org/10.5194/essd-2026-501
Preprint. Discussion started: 22 July 2026

2025 when also AW are observed in the MAP site. Summer 2025 cannot be completely described because of the survey stops in late June, and the frequency are not exhaustive.

- Autumn: This season is generally characterised by very high salinity variability (SA = 33.09–35.13 g kg^{-1}) and frequent SW, especially in 2020 and 2021 (66 and 29% respectively). Water masses reach the minimum densities during this season with an average range between 26.85 to 27.46 kg m^{-3}. IW varies from 33 to 80% increasing from 2020 to 2024 and Atlantic type waters have a frequency between 0.19 and 24%.
- Seasonal T–S: Winter variability aligns strongly with temperature and spring ranges are limited to prevailing dense LW, ArW and WCW; summer shows the dominance of strong temperature gradients across the IW domain; autumn variability aligns with salinity, and low-density surface waters, SW, dominate this season due to the strong freshwater discharge from the Bayelva river.

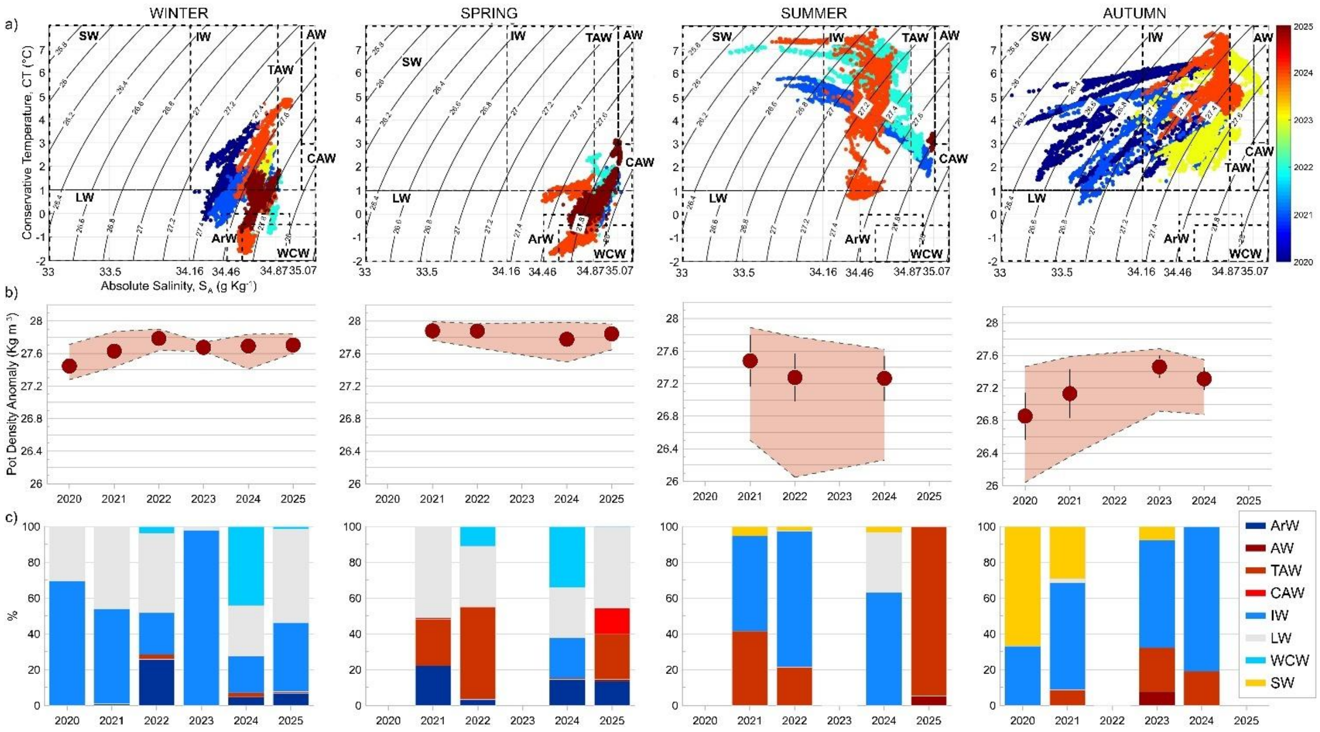

Figure 12. MAP mooring; a) TS diagram during different seasons; color coding represents the different years; b) annual variability of potential density anomaly during different seasons; c) annual variability of water mass frequencies during different seasons. (ArW: Arctic Water; AW: Atlantic Water; TAW: Trasformed Atlantic Water; CAW: Cooled Atlntic Water; IW: Intermediate Water; LW: Local Water; WCW: Winter Cooled Water; SW: Surface Water)

MDI (inner Kongsfjorden)

- Winter: we observe a strong thermohaline variability with Intermediate Waters (IW) prevailing. Minimum and maximum CT were measured in 2024 (−1.78 –5.04 °C) and SA between 34.31 and 35.09 g kg^{-1} with maximum reached in

https://doi.org/10.5194/essd-2026-501
Preprint. Discussion started: 22 July 2026

2024 and minimum in 2020. IW dominates between 2020 and 2023 while in 2024 and 2025 prevailing water masses were WCW and LW. Average density anomaly is in the range between 27.59 and 27.72 kg m^{-3}. Year 2020 shows the largest variability testified also by the more balanced presence of different water masses, while winter 2021 and 2023 were dominated by IW and LW that together account more than 93%. Atlantic-type water masses (TAW) have an alternating recurrence between the years in a range of 4% (2023) and 29% (2022).

- Spring: Variability is reduced, accompanied by an increase in the average density of water masses to values between 27.8 and 28 kg m^{-3}. Minimum CT (−1.76°C) is measured in 2023 and maximum (2.80 °C) in 2025, while salinity varies between 34.65 (2024) and 35.20 g kg^{-1} (2025). LW and WCW are the prevailing water masses that together account for more than 60% and ArW and TAW represent the minor water masses type. TAW has a maximum frequency of 21% observed in 2025.
- Summer: TAW dominates with frequency more than 70% except for 2024 when the Atlantic type waters do not inflow in the fjord and prevailing IW and LW occurred. Average density anomaly fluctuates between 27.58 and 27.73 kg m^{-3} with minimum observed during 2024, which was an exceptional fresher summer compared to other years. During summer in every year the observed variability is primarily thermal driven and interannual CT ranges were larger than 3 °C in 2020, 2022, 2023 and minimum 2021 (1.67 °C).
- Autumn: this is the warmest season with enhanced salinity variability; IW and TAW dominate throughout the study period. Indeed, in 2022 and 2023, TAW accounts for more than 80% of the observations. Furthermore, in 2023, AW intrudes into the inner fjord reaching the MDI station. Water masses exhibit the lowest mean density of the year, ranging between 27.35 and 27.59 kg m^{-3}. Autumn 2021 was characterised by lower seawater temperatures (average CT 4.43°C and minimum of 2.51°C), while 2024 was the warmest and freshest year with prevailing IW (77%). In 2023, the stronger Atlantic influence caused largest saline increase (mean SA = 35 and maximum 35.13 g kg^{-1}).
- Seasonal T–S: we observe high temperature–salinity variability during winter with prevailing IW and LW, while in spring density increases with prevailing ArW, LW and WCW. In summer and autumn, the density progressively decreases, and variability aligns predominantly along the temperature and salinity axes, respectively, with the dominance of TAW in summer and IW in autumn. This reflects temperature-driven variability in summer and freshwater-controlled modulation of salinity in autumn when lighter water masses are observed in the fjord.

https://doi.org/10.5194/essd-2026-501
Preprint. Discussion started: 22 July 2026

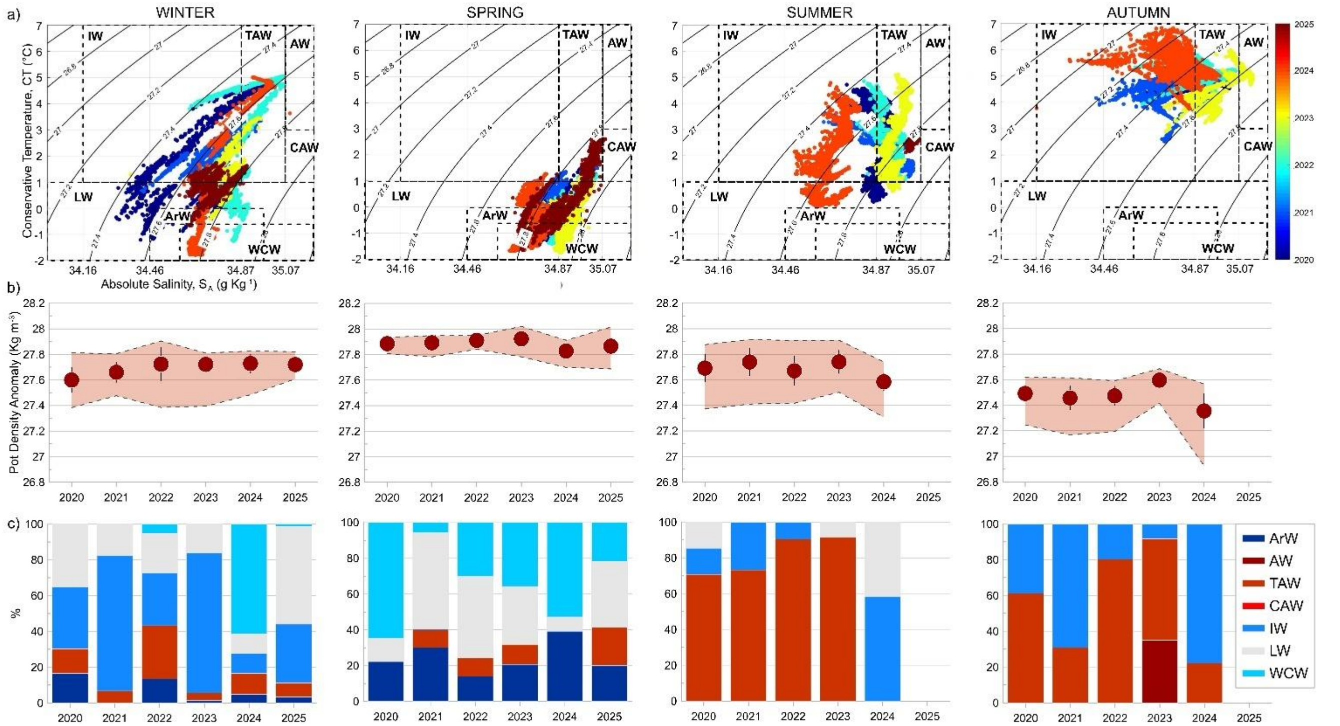

Figure 13. MDI mooring; a) TS diagram during different seasons; color coding represents the different years; b) annual variability of potential density anomaly during different seasons; c) annual variability of water mass frequencies during different seasons. (ArW: Arctic Water; AW: Atlantic Water; TAW: Transformed Atlantic Water; CAW: Cooled Atlantic Water; IW: Intermediate Water; LW: Local Water; WCW: Winter Cooled Water)

S1 (Fram Strait, offshore deep)

This site, located offshore, lies within the interaction zone between warm northward-flowing AW and cold NSDW.

- Winter: there is strong variability in temperature (and, in 2020, also salinity) in the near-bottom 200m of the water column, while the mean density anomaly of the water masses remains within a narrow range between 28.02 and 28.06 kg m^{-3}. AW dominates with more than 50% of frequency except 2022 and 2023 when frequency of NSDW is 50%. CT range is −0.90 and 3.77 °C and SA is 34.93 and 35.17 g kg^{-1}.
- Spring: thermohaline variability is reduced (CT = −1.02 to 2.94 °C; SA = 35.03–35.15 g kg^{-1}) and density anomaly ranges between 28.04 and 28.06 kg m^{-3}. Except 2021 when AW recur for the 60% of the time, NSDW prevails with frequency greater than 54%.
- Summer: variability further decreases (CT = −0.89 to 2.06 °C; SA = 35.01–35.15 g kg^{-1}) and mean density anomaly is in a range of 28.05 and 28.06 kg m^{-3} and reaches the maximum values observed during the different seasons (28.14 kg m^{-3}); NSDW remain the prevailing water mass with frequency between 57 and 75 %.

https://doi.org/10.5194/essd-2026-501
Preprint. Discussion started: 22 July 2026

- Autumn: variability increases and is primarily driven by temperature, (−0.89 to 3.29 °C), whereas salinity remains within a narrow interval (SA = 35.05–35.17 g kg^{-1}). The mean density anomaly decreases, and it is enclosed in a range of 28.04 - 28.06 kg m^{-3}. AW recurs for 64 and 55% of the time during 2020 and 2021, while during 2022 and 2023 NSDW prevails with frequencies of 60 and 61%.
- Seasonal T–S: the diagram consistently shows temperature-dominated variability that modulates the water mass density, with maxima during spring and summer and minimum during autumn and winter. 2020 is the year with different behaviour compared to other years with a greater thermohaline variability especially during winter.

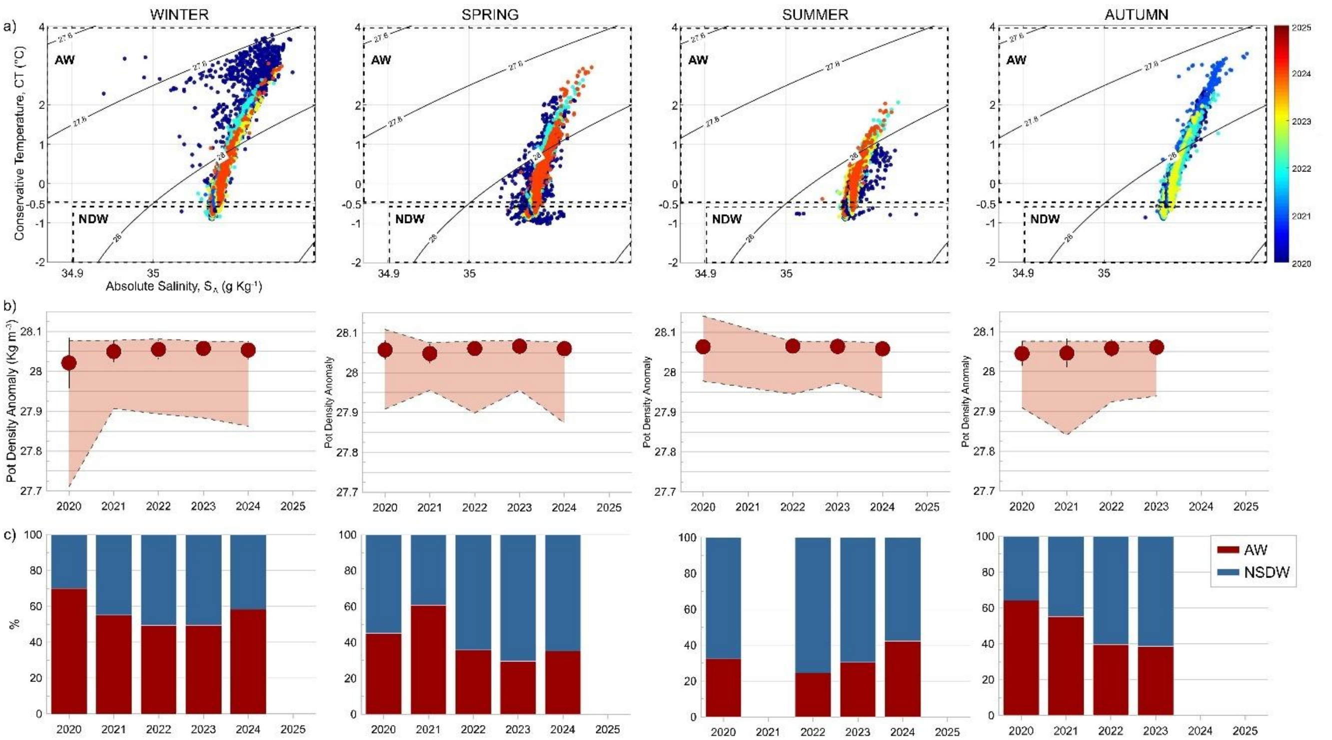

Figure 14. S1 mooring; a) TS diagram during different seasons; color coding represents the different years; b) annual variability of potential density anomaly during different seasons; c) annual variability of water mass frequencies during different seasons. (AW: Atlantic Water; NSDW: Norwegian Sea Deep Water).

8 Discussions

8.1 Hydrodynamics

In this work we have presented the dataset collected by the Italian Arctic Marine Observing system established in Svalbard since 2020 with the present configuration composed of three coastal sites and one offshore. The dataset produced by the observatory provides synoptic insights into the hydrographic variability of Svalbard fjords representing, to the best of our knowledge, one of the most spatially comprehensive, multi-sensor records currently available for the Svalbard fjord continental margin system. By integrating observations across contrasting hydrographic settings (in fjords and deep-ocean), the dataset captures dynamic processes for understanding and detecting climate change signals and their variability across scales. Such multiscale, co-located time series remain sporadic in the Arctic, where logistical constraints often limit long-term continuity; and these observing nodes are fully complementary to the long-term Svalbard Marine Observatories developed in this Arctic region and participating to the Svalbard Integrated Observing System (SIOS) to understand complex ocean processes in this rapidly changing region (Bensi et al., 2025) at both short and long-term scale.

The coordinated mooring configuration allows users to compare hydrodynamic regimes across fjord compartments that differ in geomorphology and exposure with fjord circulation strongly controlled by the interplay between basin morphology, wind forcing, and tidal dynamics (Skogseth et al., 2020; Kanarik et al., 2025). Despite past efforts on characterizing the dynamics of Kongsfjorden - Krossfjorden system, at present continuous and synoptic observations in both fjords does not exist and this work highlights the high small-scale variability within a system apparently homogeneous.

In Krossfjorden, KIM site, placed close to the fjord entrance, shows hydrodynamic regimes that follow the fjord geometry, and morphology, and current speed is susceptible to the seasonal wind regime with pronounced vertical variability. The hydrodynamic measurements revealed a highly variable seasonal pattern, with the water column alternatively characterized by layers exhibiting opposing flow directions, by a dominant flow direction that rotates with depth, or by a hydrodynamic regime primarily characterised by a vertical velocity gradient. The observations are limited to the deeper half water column and are in progress measurements to investigate the hydrodynamics of the upper half water column. Moving upward along the water column the currents are mainly in-fjord oriented.

Generally, moving landward within an Arctic fjord, the upper layer circulation is progressively less dominated by the wind (Svedsen et al., 2002; Skogset et al., 2007) which primarily influence the outflow intensity of surface water depending on the wind direction (Skogseth et al. 2007) and the hydrographic response lag the wind forcing from hours to days depending on the fjord morphology and thickness of the surface layer (Cottier et al., 2005; Skarðhamar & Svendsen, 2010). Moving into Kongsfjorden, in the shallow MAP site, the seasonal evolution of currents is related to the seasonality of wind patterns, but direction of the flow remains with a dominant direction strongly controlled by coastal morphology with resulting dominant alongshore currents (Repp, 1988). In the inner-fjord site, MDI, the currents exhibit persistently weak magnitudes (0.01 -- 0.05 m s-1) and strong bidirectionality aligned with the fjord axis without defined vertical variability. The observed hydrodynamics, measured in this inner part after the Blomstrandhalvøya, is the result of complex interaction between baroclinic and barotropic flow (Nilsen et al., 2016, Janzen et al., 2005; Svendsen et al., 2002), where the mean circulation patterns is modulated by Coastal Trapped Waves (Inall et al., 2015), and the contribution of weak tides on the total velocities is poorly relevant (Svendsen et al., 2002; Cottier et al., 2010). Seasonal hydrodynamic patterns can be explained with seasonal evolution of the shelf - fjord density gradients (Cottier et al., 2005; Klinck et al., 1981; Svendsen et al., 2002; Sundfjord et al., 2017). The main outflow observed at depth during winter, and spring can be addressed to typical cold months when density in the fjord is great and generally larger that on the shelf. On the contrary, during summer and autumn, the higher frequency of the inflowing currents in the upper layers can be attributable to the large amounts of freshwaters discharged from glaciers which reduces water density in the fjord and weakens the geostrophic control mechanism, thereby facilitating inflow into the fjord.

The deep-ocean mooring S1 reveals a persistent NW–SE bidirectional flow typical of the slope current system, including seasonal modulation of intensity and deep-layer pulses that align with previously observed internal-wave and topographically guided flow features (Bensi et al., 2019). The measurements reveal vigorous deep current activity along the depth layer between 545 and 1000m depth. Several times, we observed along-slope strong pulsation exceeding 0.4 ms-1. The prevailing direction was directed north-westward especially above 700m with periodical inversion of the flow recurring mainly during wintertime. Bensi et al., (2019) found an overall consistency between the variability of the deep-sea currents and the local wind variation especially on seasonal and short temporal scales. The presence of strong hydrodynamics in the deep layer was already found in previous experiments where Sanchez-Vidal et al., (2015) observed higher turbidity in the near-bottom layer due to sediment resuspension at 1500 m depth along the west Spitsbergen continental slope. The wintertime is characterised by favourable low-pressure atmosphere systems that influence the West Spitsbergen Shelf area (Nielsen et al., 2021) and sporadic currents coming from north are addressed mainly to the action of northerly winds and heat loss on the shelf that trigger the arrival of gravity currents driven by dense water plumes formed over the shelf or formed after sea ice formation within the fjords and polynyas. The continuous measurements at 500–1000 m depth provide a rare long-term record of deep boundary current dynamics in the Fram Strait, a region critical for monitoring exchanges between the Atlantic and Arctic oceanic basins. For climate and circulation studies, these observations are of value because deep boundary current datasets in Arctic waters are exceptionally scarce.

8.2 Thermohaline and Water-Mass variability

Across all sites, the dataset captures consistent seasonal phasing of temperature and salinity, with pronounced vertical variability and influenced by proximity to freshwater sources. The seasonal fluctuation of density anomaly is one of the factors triggering the baroclinic currents between the shelf and fjord (Tverberg et al., 2019). In the fjords, moorings resolve sharp summer freshening and warming in upper layers, reflecting glacial melt, river discharge, and seasonal solar-induced stratification. Conversely, winter conditions reveal denser, colder waters with enhanced homogeneity (i.e., mixing) throughout the water column. Years exhibiting the highest temperatures during the late-summer and autumn period (September - October) correspond to those with the most intense Atlantic waters intrusions.

At KIM in Krossfjorden, heat accumulated during summer propagates from the surface down to ~150–200 m in early autumn, when the surface layer starts cooling again. Salinity shows lower variability between the two depth levels (-65 and -120m), but is consistently lower in the upper layer. In Kongsfjorden, the thermal structure and variability at shallow site are weaker, whereas a pronounced vertical salinity gradient persists even in shallow waters. Fresher surface layers result from glacier-derived freshwater input from both tidewater and land-terminating glaciers (Ingrosso et al., 2025; Scholzen et al., 2021; De Rovere et al., 2025). This freshwater input promotes seasonal stratification, enhancing along-fjord circulation (Ingvaldsen et al., 2001; Straneo & Cenedese, 2015; Sundfjord et al., 2017; Stigebrandt, 2012). This condition, together with density

https://doi.org/10.5194/essd-2026-501
Preprint. Discussion started: 22 July 2026

variations on the shelf, generated by regional wind patterns that drive Ekman transport (Klinck et al., 1981; Stigebrandt, 1981, 2012; Svendsen, 1980; Cottier et al., 2007), modulate shelf-fjord exchange. These typical summer and autumn conditions can facilitate the advection of Spitsbergen Trough Current, promoting the inflow of AW into the fjords breaking the geostrophic control of shelf circulation (Nilsen et al., 2016; Tverberg et al., 2019). However, AW intrusions may also occur during winter, depending on the different winter circulation scenarios defined by Tvergerg et al. (2019) and on the advection of anomalously low-salinity waters from the northern Barents Sea onto the West Spitsbergen Shelf (De Rovere et al., 2024).

Our data document substantial seasonal and interannual variability of the seawater properties framing a synoptic overview of water masses as well as density variations. The presence of AW and TAW at inner-fjord sites during multiple summers and autumns, as well as their episodic penetration into shallower waters at MAP site, provides a clear evidence of recurring AW intrusions and reinforce tendency toward a major Atlantic-type of fjord initiated after 2006 in the western fjords of Spitsbergen (Tverberg et al., 2019; Skogseth et al., 2020; Polyakov et al., 2017; Ingvaldsen et al., 2021). In the Kross-Kongsfjorden system the Krossfjord is largely affected by the AW intrusions, being more exposed to offshore waters influence.

Although the uppermost temperature sensor on mooring S1 is located at the base of the AW core, the entire offshore time series shows seasonal variability, with Atlantic waters penetrating more deeply into the bottom layer in autumn and winter. This is primarily due to increased energy input from atmospheric phenomena, in these seasons, which triggers internal oscillations that can cause the AW to sink below a depth of 800 m (Bensi et al., 2019). This phenomenon seems linked to large-scale processes such as the general intensification of NAO and consequent atmospheric events (Lien at al. 2014). In particular, the internal oscillation is amplified by the passage of high-low atmospheric pressure systems extending its influence from the surface down to the deep layers. Thermohaline variability is associated with vigorous deep-current activity between 545 and 1000m depth, while the thermohaline structure of the water column is modulated by wind forcing, the effects of which extend to the deep layers.

Marine observations collected over the last five year highlight the relatively low variability of offshore deep-water dynamics compared to those observed in the Krossfjorden-Kongsfjorden system, punctuated by oscillations linked to large scale circulation and atmospheric processes. Indeed, in the coastal systems, dynamics arise from a more complex interplay of atmospheric, hydrological, and hydrographic factors that amplify both short-term and seasonal variations. The combination of high temporal resolution, vertical and horizontal data distribution allows robust characterization and comparison among water-masses variability in the offshore, shelf, and fjord environments. Beyond individual deployments, the scientific value of the dataset lies in its ability to resolve how physical anomalies propagate horizontally and vertically under changing atmospheric forcing and shelf conditions. The water-mass classifications, combined with continuous CT and S_A records, provide robust indicators of extreme events possibly associated with climatic signals, which are not always easy to discern without continuous measurements.

https://doi.org/10.5194/essd-2026-501
Preprint. Discussion started: 22 July 2026

8.3 Dataset Reliability and scientific reuse

The dataset represents a key resource for the international Arctic research community and will support ongoing assessments of climate-sensitive processes in the Svalbard region. Rigorous quality-control procedures—based on standardized test sequences and SeaDataNet-compliant flagging—ensure internal consistency and long-term comparability across deployments. Owing to its interoperability the dataset is readily reusable across a broad range of scientific and operational applications. These include evaluating subsurface heat supply to tidewater glaciers, detecting Atlantification trends across fjord compartments and depth layers, validating regional- to basin-scale ocean circulation models, and integrating sedimentary, biogeochemical, and ecological observations from SIOS and other Arctic observatories. In a broader context, our data contribute to a long-term assessments of Arctic and Atlantic water-mass variability relevant to studies of the Atlantic Meridional Overturning Circulation (AMOC) and Arctic Ocean Circulation (ArOC), while reducing the need for additional field campaigns and supporting sustainable observational strategies in polar environments.

9 Conclusions

At present, most Arctic observational data records are dispersed across numerous institutions and locations, often stored in heterogeneous formats and media, with significant duplication or near duplication and multiple data versions. The absence of a coordinated pan-Arctic data aggregation system makes the aggregation, integration, and effective use of these globally distributed datasets highly labour-intensive and dependent on specialized expertise (Simoncelli et al., 2025). Currently, SIOS is the main research infrastructure at Svalbard undertaking systematic aggregation efforts, collecting new or updated data from multiple sources into a harmonized, searchable, and well documented framework (Christiansen et al., 2024). However, this activity remains geographically limited to the Svalbard area and does not yet constitute a comprehensive pan-Arctic solution. The Italian Arctic Marine Observing system contributes to the SIOS Marine Infrastructure Network providing high temporal-resolution, multi-year dataset that significantly advances observational capacity in the Svalbard region and contribute to the Arctic-Atlantic Distributed Biological Observatory (A-DBO). The approach used enhances the scientific value of research outputs, supports international collaboration, and safeguards intellectual property rights, while maximizing the economic and social value of data. By spanning diverse hydrographic coastal environments from different tidewater glaciers (freshwater sources) to deep Atlantic pathways, the dataset enables an unprecedented synoptic overview of both local and regional ocean dynamic processes. Our data document robust seasonal cycles, episodic warm-water intrusions, interannual variability in water masses, and strong spatial gradients shaped by coastal geomorphology and shelf connectivity. They are a key component for evaluating the progression of climate change processes, quantifying heat and salt exchanges between fjords and the open-ocean and supporting long-term model validation efforts. The Italian marine Observing System is fully complementary to the other Arctic marine observatories, and it is a distributed node that can sustain the development of the Arctic observing and data system infrastructure. The continuation of the observatory's activities will enable a deeper understanding of hydrographic

https://doi.org/10.5194/essd-2026-501
Preprint. Discussion started: 22 July 2026

variability in the Arctic and will serve as a milestone for collaborative research and the creation of an integrated, interoperable, and accessible Arctic observation system.

Data availability

All datasets generated by the Italian Arctic Marine Observing system are fully compliant with FAIR principles with open and free availability through the Italian Arctic Data Centre (IADC, https://metadata.iadc.cnr.it/). and stored and accessible in the ERDDAP archive. DOI assignment of each dataset is provided via the DataCite service integrated within the IADC metadata portal. The full list of datasets is available through the ERDDAP page ((https://data.iadc.cnr.it/) and for each dataset is provided a DOI. The full list of datasets is reported below:

KIM MOORING	
DATASET	**DOI**
KIM Mooring CTD data @ 65m (Paladini de Mendoza et al., 2025a)	https://doi.org/10.71761/273db33e-608f-4467-9ba4-59405833f716
KIM Mooring CTD data @ 120m (Paladini de Mendoza et al., 2025b)	https://doi.org/10.71761/edcfcfea-397e-4ea2-ac33-b4ed324440c0
KIM Mooring T data @ 180m (Paladini de Mendoza et al., 2025c)	https://doi.org/10.71761/518150fb-b5a5-4530-bd54-fc973712083a
KIM Mooring ADCP data @ 200m (Paladini de Mendoza et al., 2025e)	https://doi.org/10.71761/36bbf408-ab4d-4c84-aced-614827df0e0a
KIM Mooring T data @ 300m (Paladini de Mendoza et al., 2025d)	https://doi.org/10.71761/90247d99-32b2-43d0-b290-d77d09238b27
MDI MOORING	
MDI Mooring CTD data @ 27m (Paladini de Mendoza et al., 2024a)	https://doi.org/10.53132/CNR-ISP.2024.DAT.GCC.OCE.ART.52
MDI Mooring T data @ 50m (Paladini de Mendoza et al., 2025f)	https://doi.org/10.71761/77854a27-5f8e-401f-ac61-09ba95a6ce25
MDI Mooring T data @ 65m (Paladini de Mendoza et al., 2025g)	https://doi.org/10.71761/85ec45e1-d54d-4f91-9fa5-67c5f4e33f69
MDI Mooring CTD data @ 89m (Paladini de Mendoza et al., 2024b)	https://doi.org/10.53132/CNR-ISP.2024.DAT.GCC.OCE.ART.54
MDI Mooring ADCP data @ 95m (Paladini de Mendoza et al., 2025h)	https://doi.org/10.71761/143c4fe0-42b7-4acb-893a-87671f3410aa

https://doi.org/10.5194/essd-2026-501
Preprint. Discussion started: 22 July 2026

MAP MOORING	
MAP Mooring CTD and SeaFet data at 20m (Paladini de Mendoza et al., 2026a)	10.71761/73e04bc5-e9c5-4bf6-99e4-c19df6bb5a34
MAP Mooring CTD data @ 35m (Paladini de Mendoza et al., 2026b)	https://doi.org/10.71761/263078b8-81d3-4749-aeb3-0e0cbad3c02b
MAP mooring Aquadopp data at 35m (Paladini de Mendoza et al., 2026c)	https://doi.org/10.71761/0e4fb042-a689-41fa-8baf-769067dd1d87
MAP Mooring T data @ 40m (Paladini de Mendoza et al., 2026d)	https://doi.org/10.71761/fa6b4a97-1688-4057-9914-8fc72c5134e3
S1 MOORING	
S1 Mooring ADCP downward looking data @ 782 - 740 - 488m (Paladini de Mendoza et al., 2026e)	https://doi.org/10.71761/4ca9d498-de6f-46ad-8654-72732116157e
S1 Mooring TS data @ 785m (Paladini de Mendoza et al., 2026f)	https://doi.org/10.71761/f92c6985-0315-4236-a1ba-367a2c4a0b2b
S1 Mooring TS data @ 820m (Paladini de Mendoza et al., 2026g)	https://doi.org/10.71761/ce81e931-7221-4483-956a-cf0ea94cbf04
S1 Mooring T data @ 893m (Paladini de Mendoza et al., 2026h)	https://doi.org/10.71761/b919a98e-c90c-454e-ab5b-33c67f0ea0e6
S1 Mooring TS data @ 940m (Paladini de Mendoza et al., 2026i)	https://doi.org/10.71761/919c71e6-69d9-4880-ad49-6a5f0fb784ee
S1 Mooring T data @ 970m (Paladini de Mendoza et al., 2026l)	https://doi.org/10.71761/37d890b9-e337-407f-bc65-585da9742127
S1 Mooring TS data @ 1000m (Paladini de Mendoza et al., 2026m)	https://doi.org/10.71761/870f09b5-68e3-495b-8d91-7baa30f02198
S1 Mooring single point current meter data @ 1000m (Paladini de Mendoza et al., 2026n)	https://doi.org/10.71761/d08eea94-b532-47a0-93c1-a321cc0ea6b2
S1 Mooring T data @ 1020m (Paladini de Mendoza et al., 2026o)	https://doi.org/10.71761/cf62771e-39d4-459c-81cc-1469f51a1516

Author contributions

SM, LL, MB, FG, TT designed the Italian Marine Arctic Observatory; SM, LL, FPdM, TT, GI, PG, FG maintain the observatory and carry out fieldwork activities; FPdM write the original draft; FPdM, MB, LP analysed the data and prepared the figures. FPdM prepared the submitted form of the manuscript with contributions from all co-authors. AC, GV, MM and CR planned and realise the IADC data portal and the ERDAPP data archive.

Competing interests

The authors declare that they have no conflict of interest.

Disclaimer

Copernicus Publications remains neutral with regard to jurisdictional claims made in the text, published maps, institutional affiliations, or any other geographical representation in this paper. While Copernicus Publications makes every effort to include appropriate place names, the final responsibility lies with the authors. Views expressed in the text are those of the authors and do not necessarily reflect the views of the publisher."

Acknowledgements

The authors are grateful to the support given by the KingsBay for the Kong-Krossfjorden fieldwork activities and logistic in NyAlesund Research Station and by the personnel and management team of the Italian Arctic Station "Dirigibile Italia" in supporting researchers during the stay in NyAlesund. For the S1 mooring maintenance, thanks are also due to the personnel (crew and technicians) of the RV Alliance (cruises 2017-2025), managed by the Italian Navy Hydrographic Institute (High North programme) and NATO Science and Technology Organization, Centre for Maritime Research and Experimentation and to the personnel of the IB Laura Bassi (cruise 2021), managed by the OGS, Trieste, Italy. The authors thanks also Vito Vitale for its fundamental contribute to the design and realization of IADC data portal.

Financial support

The activities related to the upgrade and maintenance of MDI, S1 and KIM moorings and the development of IADC data portal have been funded by the EU— Next Generation EU Mission 4, Component 2—CUP B53C22002150006 —Project IR0000032–ITINERIS—Italian Integrated Environmental Research Infrastructures System, project PRIN 2022/2022CCRN7R – "ATTRACTION" and Arctic Research Program for Research Infrastructures project, (PRA INFRA), iMOS#2024. The mooring MAP management has been conducted thanks to the financial support of the Joint Research Centre ENI-CNR

https://doi.org/10.5194/essd-2026-501
Preprint. Discussion started: 22 July 2026

"AldoPontremoli" and the Svalbard Science Forum (SSF) for the Arctic Field Grant "Monitoring seawater CO_2 release from thawing permafrost mobilized by Bayelva proglacial stream" project (RiS ID 11654; NFR contract 333041, 350607, 356537).

References

Aliani, S., Bartholini, G., Degl'innocenti, F., Delfanti, R., Galli, C., Lazzoni, E., et al.: Multidisciplinary investigations in the marine environment of the inner Kongsfiord, Svalbard islands (September 2000 and 2001). Chemistry and Ecology, 20(sup1), S19–S28. https://doi. org/10.1080/02757540410001655396, 2004.

Bensi, M., Kovačević, V., Langone, L., Aliani, S., Ursella, L., Goszczko, I., Soltwedel, T., Skogseth, R., Nilsen, F., Deponte, D., Mansutti, P., Laterza, R., Rebesco, M., Rui, L., Lucchi, R. G., Wåhlin, A., Viola, A., Beszczynska-Möller, A., & Rubino, A. Deep Flow Variability Offshore South-West Svalbard (Fram Strait). Water, 11(4), 683. https://doi.org/10.3390/w11040683, 2019.

Bensi M, Kovacevic V, Langone L, Miserocchi S, Demarte M, Ivaldi R: Spitsbergen Oceanic and Atmospheric interactions.In: Van den Heuvel et al (eds) SESS report 2019, Svalbard Integrated Arctic Earth Observing System, Longyearbyen, pp 250-261 https://doi.org/10.5281/zenodo.4777750, 2020.

Bensi M, Nilsen F, Bénédicte F, Skogseth R, Moskalik M, Korhonen M, Vogedes D, Kovacevic V, Paladini de Mendoza F, Ingrosso G, Langone L, Giordano P, Inall M, Mano B, Sundfjord A Bailey A, Foss Ø, Daase M, Castro de la Guardia L, Jones E,: The Atlantification process in Svalbard: a broad view from the SIOS Marine Infrastructure network. In: Runge et al (eds) SESS report 2024, Svalbard Integrated Arctic Earth Observing System. doi: 10.5281/zenodo.14425673, (2025).

Carmack, E., & Aagaard, K.: On the deep water of the Greenland Sea. Deep Sea Research and Oceanographic Abstracts, 20(8), 687–715. https://doi.org/10.1016/0011-7471(73)90086-7, 1973.

Carmack, E., et al.: Towards quantifying the increasing role of oceanic heat in sea ice loss in the new Arctic, Bull. Am. Meteorol. Soc., doi:10.1175/BAMS-D-13-00177.1, 2015a.

Christiansen, H. H., Matero, I. S. O., Baddeley, L., Holmén, K., Hoppe, C. J. M., Loonen, M. J. J. E., Storvold, R., Vitale, V., Zaborska, A., and Lihavainen, H.: Developing the Svalbard Integrated Arctic Earth Observing System (SIOS), Earth Syst. Dynam., 15, 933–946, https://doi.org/10.5194/esd-15-933-2024, 2024.

Chylek, P., C. K. Folland, G. Lesins, M. K. Dubey, and M. Wang: Arctic air temperature change amplification and the Atlantic Multidecadal Oscillation, Geophys. Res. Lett., 36, L14801, doi:10.1029/2009GL038777, 2009.

Comiso, J. C.: Large Decadal Decline of the Arctic Multiyear Ice Cover. J. Climate, 25, 1176–1193, https://doi.org/10.1175/JCLI-D-11-00113.1, 2012.

Coppola, L., Ntoumas, M., Bozzano, R., Bensi, M., Hartman, S. E.,Charcos Llorens, Mi., Craig, J., Rolin, J-F., Giovanetti, G., Cano, D., Karstensen, J., Cianca, A., Toma, D., Stasch, C., Pensieri, S., Cardin, V., Tengberg, A., Petihakis, G., Cristini, L.: Handbook of best practices for open ocean fixed observatories. European Commission, FixO3 Project, 127pp. (European

Commission, FixO3 project, FP7 Programme 2007-2013 under grant agreement n° 312463). https://doi.org/10.25607/OBP-1488, 2016.

Cottier, F. R., Nilsen, F., Inall, M. E., Gerland, S., Tverberg, V., and Svendsen, H.: Wintertime warming of an Arctic shelf in response to large-scale atmospheric circulation. Geophys. Res. Lett. 34:L10607, https://doi.org/10.1029/2007GL029948, 2007.

Cottier, F. R., F. Nilsen, R. Skogseth, V. Tverberg, J. Skardhamar, and H. Svendsen: Arctic fjords: A review of the oceanographic environment and dominant physical processes, Geol. Soc. Spec. Publ., 344, 51–60, https://doi.org/10.1144/SP344.4, 2010.

DataCite Metadata Working Group: DataCite Metadata Schema for the Publication and Citation of Research Data and Other Research Outputs. Version 4.6. DataCite e.V. https://doi.org/10.14454/mzv1-5b55, 2024.

D'Angelo, A., Giglio, F., Miserocchi, S., Sanchez-Vidal, A., Aliani, S., Tesi, T., Viola, A., Mazzola, M., Langone, L.: Multi-year particle fluxes in Kongsfjorden, Svalbard. Biogeosciences 15, 5343–5363, https://doi.org/10.5194/bg-15-5343-2018, 2018.

De Rovere, F., Langone, L., Schroeder, K., Miserocchi, S., Giglio, F., Aliani, S., & Chiggiato, J.: Water masses variability in inner Kongsfjorden (Svalbard) during 2010–2020. Frontiers in Marine Science, 9, 741075. https://doi.org/10.3389/fmars.2022.741075, 2022.

De Rovere, F., Zanchettin, D., Rubino, A., Langone, L., Calogiuri, F., Ruggieri, P., et al.: Winter intrusions of Atlantic Water in Kongsfjorden: Oceanic preconditioning and atmospheric triggering. Journal of Geophysical Research: Oceans, 129(7), e2023JC020095. https://doi.org/10.1029/2023jc020095, 2024.

De Rovere, F., Chiggiato, J., Langone, L., Sundfjord, A., Albretsen, J., & Duarte, P.: Changes in the coastal wind field and river runoff conditions expose Kongsfjorden (Svalbard) to the influence of Atlantic Water. Journal of Geophysical Research: Oceans, 130, e2024JC020924. https://doi.org/10.1029/2024JC020924, 2025.

Eriksen, E., Gjøsæter, H., Prozorkevich, D., Shamray, E., Dolgov, A., Skern-Mauritzen, M., Stiansen, J. E., Kovalev, Y., and Sunnanå, K.: From Single Species Surveys towards Monitoring of the Barents Sea Ecosystem, Prog. Oceanogr., 166, 4–14, https://doi.org/10.1016/j.pocean.2017.09.007, 2018.

Ha, H. K., Kim, Y. H., Lee, H. J., Hwang, P., & Joo, H. M.: Under-ice measurements of suspended particulate matters using ADCP and LISST-Holo. Ocean Science Journal, 50(1), 97, 2015a.

Ha, Ho Kyung, et al.: Variability of ADCP Backscattering Signals Captured by Long-Term Moorings: Amundsen Shelf, Antarctica. The 21st International Symposium on Polar Sciences. KOPRI, Incheon. 2015.05.19-20, 2015b.

Inall, M. E., F.Nilsen, F. R.Cottier, and R.Daae: Shelf/fjord exchange driven by coastal-trapped waves in the Arctic, J. Geophys. Res. Oceans, 120, 8283–8303, doi:10.1002/2015JC011277, 2015.

Infrastrutture di ricerca e siti osservativi. Rapporto annuale 2023.AUTORI VARI EDITOR: GRUPPO DI LAVORO COMUNICAZIONE CNR-ISP. https://doi.org/10.53132/CNR-ISP.2024.REP.SCI.VAR.55, 2023.

https://doi.org/10.5194/essd-2026-501
Preprint. Discussion started: 22 July 2026

Ingrosso, G., Ceccarelli, C., Giglio, F. et al: Greening of Svalbard in the twentieth century driven by sea ice loss and glaciers retreat. Commun Earth Environ 6, 30. https://doi.org/10.1038/s43247-025-01994-y, 2025.

Ingvaldsen, R., Reitan, M. B., Svendsen, H., & Asplin, L.: The upper layer circulation in Kongsfjorden and Krossfjorden-A complex fjord system on the west coast of Spitsbergen, Environmental Research in the Arctic 2000: Proceedings of the Second International Symposium on Environmental Research in the Arctic and Fifth Ny-Alesund Scientific Seminar, 23-25 February 2000. Mem. Natl. Inst. Polar Res., Spec. Issue, 54, 393–407. Tokyo: National Institute of Polar Research, 2001.

Ingvaldsen, R.B., Assmann, K.M., Primicerio, R. et al.: Physical manifestations and ecological implications of Arctic Atlantification. Nat Rev Earth Environ 2, 874–889. https://doi.org/10.1038/s43017-021-00228-x, 2021.

IOC, SCOR and IAPSO, 2010: The international thermodynamic equation of seawater - 2010: Calculation and use of thermodynamic properties. Intergovernmental Oceanographic Commission, Manuals and Guides No. 56, UNESCO (English), 196 pp. Available from http://www.TEOS-10.org See section 3.3 of this TEOS-10 Manual.

Jackett, D. R., McDougall, T. J., Feistel, R., Wright, D. G., and Griffies, S. M.: Algorithms for Density, Potential Temperature, Conservative Temperature, and the Freezing Temperature of Seawater, J. Atmos. Ocean. Tech., 23, 1709–1728, https://doi.org/10.1175/JTECH1946.1, 2006.

Janzen, C. D., J. H. Simpson, M. E. Inall, and F. Cottier: Across-sill circulation near a tidal mixing front in a broad fjord, Cont. Shelf Res., 25(15), 1805–1824, doi:10.1016/j.csr.2005.06.004, 2005.

Kanarik, H., Tuomi, L., Alenius, P., Miettunen, E., Johansson, M., Roine, T., Westerlund, A., and Kahma, K. K.: Currents and their drivers in the Archipelago Sea: insights from ADCP measurements, Ocean Sci., 21, 2125–2147, https://doi.org/10.5194/os-21-2125-2025, 2025.

Killworth, P. D.: Deep convection in the world ocean. Reviews of Geophysics and Space Physics, 21(1), 1–26. https://doi.org/10.1029/RG021i001p00001, 1983.

Klinck, J. M., J. J. O'Brien, and H. Svendsen: A simple model of fjord and coastal circulation interaction, J. Phys. Oceanogr., 11, 1612–1626, 1981.

Lien, V.S., Gusdal, Y. & Vikebø, F.B.: Along-shelf hydrographic anomalies in the Nordic Seas (1960–2011): locally generated or advective signals?. Ocean Dynamics 64, 1047–1059. https://doi.org/10.1007/s10236-014-0736-3, 2014.

Liffers, M., et al. DataCite Metadata Working Group: DataCite Metadata Schema for the Publication and Citation of Research Data and Other Research Outputs. Version 4.6. DataCite e.V. https://doi.org/10.14454/mzv1-5b55, 2024.

Lin, D., Crabtree, J., Dillo, I. et al.: The TRUST Principles for digital repositories. Sci Data 7, 144. https://doi.org/10.1038/s41597-020-0486-7, 2020.

Lind, S., Ingvaldsen, R.B. & Furevik, T.: Arctic warming hotspot in the northern Barents Sea linked to declining sea-ice import. Nature Clim Change 8, 634–639. https://doi.org/10.1038/s41558-018-0205-y, 2018.

Mazzola, M., Viola, A.P., Lanconelli, C. et al.: Atmospheric observations at the Amundsen-Nobile Climate Change Tower in Ny-Ålesund, Svalbard. Rend. Fis. Acc. Lincei 27 (Suppl 1), 7–18. https://doi.org/10.1007/s12210-016-0540-8, 2016.

McDougall, T.J. and P.M. Barker: Getting started with TEOS-10 and the Gibbs Seawater (GSW) Oceanographic Toolbox, 28pp., SCOR/IAPSO WG127, ISBN 978-0-646-55621-5, 2011.

McDougall, T. J., Jackett, D. R., Millero, F. J., Pawlowicz, R., and Barker, P. M.: A global algorithm for estimating Absolute Salinity, Ocean Sci., 8, 1123–1134, https://doi.org/10.5194/os-8-1123-2012, 2012.

Meredith, M. et al.: Polar Regions. Chapter 3, IPCC Special Report on the Ocean and Cryosphere in a Changing Climate, 2019.

Muilwijk, M., Ilicak, M., Cornish, S. B., Danilov, S., Gelderloos, R., Gerdes, R., et al.: Arctic Ocean response to Greenland Sea wind anomalies in a suite of model simulations. Journal of Geophysical Research: Oceans, 124, 6286–6322. https://doi.org/10.1029/ 2019JC015101, 2019.

Nestola et al., Assessing the adoption of the FAIR principles in Italian environmental research infrastructures, Patterns, 7, https://doi.org/10.1016/j.patter.2025.101420, 2025.

Nicolai, A., Paladini de Mendoza, F., Ingrosso, G., Langone, L., Tesi, T., Titocci, J., & Giordano, P.: Puzzles from the Arctic–deciphering temporal distribution, ecological niche and life history of two Appendicularia species in Kongsfjorden, Svalbard Islands. Frontiers in Marine Science, 12, 1664196. https://doi.org/10.3389/fmars.2025.1664196, 2025.

Nilsen, F., Skogseth, R., Vaardal-Lunde, J., & Inall, M.: A simple shelf circulation model: Intrusion of Atlantic Water on the West Spitsbergen shelf. Journal of Physical Oceanography, 46(4), 1209–1230. https://doi.org/10.1175/jpo-d-15-0058.1, 2016.

Nilsen, F., Ersdal, E. A., & Skogseth, R.: Wind-driven variability in the Spitsbergen Polar Current and the Svalbard Branch across the Yermak Plateau. Journal of Geophysical Research: Oceans, 126, e2020JC016734. https://doi.org/10.1029/2020JC016734, 2021.

OceanSITES (2020) OceanSITES Data Format Reference Manual NetCDF Conventions and Reference Tables. Version 1.4 July 16, 2020. Geneva, Switzerland, OceanSITES, JCOMMOPS, 36pp. DOI: http://dx.doi.org/10.25607/OBP-421.2

Paladini de Mendoza F., Schroeder K., Langone L., Chiggiato J., Borghini M., Giordano P., et al.: Deep-water hydrodynamic observations of two moorings sites on the continental slope of the southern Adriatic sea (mediterranean sea). Earth Sys. Sci. Data14, 5617–5635. doi: 10.5194/essd-14-5617-2022, 2022.

Paladini de Mendoza F. et al.: MDI Mooring CTD data @ 27m [data set]. https://doi.org/10.53132/CNR-ISP.2024.DAT.GCC.OCE.ART.52, 2024a.

Paladini de Mendoza F. et al.: MDI Mooring CTD data @ 89m [data set]. https://doi.org/10.53132/CNR-ISP.2024.DAT.GCC.OCE.ART.54, 2024b.

Paladini de Mendoza F. et al.: KIM Mooring CTD data @ 65m [data set]. https://doi.org/10.71761/273db33e-608f-4467-9ba4-59405833f716, 2025a.

Paladini de Mendoza F. et al.: KIM Mooring CTD data @ 120m [data set]. https://doi.org/10.71761/edcfcfea-397e-4ea2-ac33-b4ed324440c0, 2025b.

Paladini de Mendoza F. et al.: KIM Mooring T data @ 180m [data set]. https://doi.org/10.71761/518150fb-b5a5-4530-bd54-fc973712083a, 2025c.

Paladini de Mendoza F. et al.: KIM Mooring T data @ 300m [data set]. https://doi.org/10.71761/90247d99-32b2-43d0-b290-d77d09238b27, 2025d.

Paladini de Mendoza F. et al.: KIM Mooring ADCP data @ 200m [data set]. https://doi.org/10.71761/36bbf408-ab4d-4c84-aced-614827df0e0a, 2025e.

Paladini de Mendoza F. et al.: MDI Mooring T data @ 50m [data set]. https://doi.org/10.71761/77854a27-5f8e-401f-ac61-09ba95a6ce25, 2025f.

Paladini de Mendoza F. et al.: MDI Mooring T data @ 65m [data set]. https://doi.org/10.71761/85ec45e1-d54d-4f91-9fa5-67c5f4e33f69, 2025g.

Paladini de Mendoza F. et al.: MDI Mooring ADCP data @ 95m [data set]. https://doi.org/10.71761/143c4fe0-42b7-4acb-893a-87671f3410aa, 2025h.

Paladini de Mendoza F. et al.: MAP Mooring CTD and SeaFet data at 20m [data set]. https://doi.org/10.71761/73e04bc5-e9c5-4bf6-99e4-c19df6bb5a34, 2026a.

Paladini de Mendoza F. et al.: MAP Mooring CTD data @ 35m [data set]. https://doi.org/10.71761/263078b8-81d3-4749-aeb3-0e0cbad3c02b, 2026b.

Paladini de Mendoza F. et al.: MAP mooring Aquadopp data at 35m [data set]. https://doi.org/10.71761/0e4fb042-a689-41fa-8baf-769067dd1d87, 2026c.

Paladini de Mendoza F. et al.: MAP Mooring T data @ 40m [data set]. https://doi.org/10.71761/fa6b4a97-1688-4057-9914-8fc72c5134e3, 2026d.

Paladini de Mendoza F. et al.: S1 Mooring ADCP downward looking data @ 782 - 740 - 488m [data set]. https://doi.org/10.71761/4ca9d498-de6f-46ad-8654-72732116157e, 2026e.

Paladini de Mendoza F. et al.: S1 Mooring TS data @ 785m [data set]. https://doi.org/10.71761/f92c6985-0315-4236-a1ba-367a2c4a0b2b, 2026f.

Paladini de Mendoza F. et al.: S1 Mooring TS data @ 820m [data set]. https://doi.org/10.71761/ce81e931-7221-4483-956a-cf0ea94cbf04, 2026g.

Paladini de Mendoza F. et al.: S1 Mooring T data @ 893m [data set]. https://doi.org/10.71761/b919a98e-c90c-454e-ab5b-33c67f0ea0e6, 2026h.

Paladini de Mendoza F. et al.: S1 Mooring TS data @ 940m [data set]. https://doi.org/10.71761/919c71e6-69d9-4880-ad49-6a5f0fb784ee, 2026i.

Paladini de Mendoza F. et al.: S1 Mooring T data @ 970m [data set]. https://doi.org/10.71761/37d890b9-e337-407f-bc65-585da9742127, 2026l.

Paladini de Mendoza F. et al.: S1 Mooring TS data @ 1000m [data set]. https://doi.org/10.71761/870f09b5-68e3-495b-8d91-7baa30f02198, 2026m.

Paladini de Mendoza F. et al.: S1 Mooring single point current meter data @ 1000m [data set]. https://doi.org/10.71761/d08eea94-b532-47a0-93c1-a321cc0ea6b2, 2026n.

https://doi.org/10.5194/essd-2026-501
Preprint. Discussion started: 22 July 2026

Paladini de Mendoza F. et al.: S1 Mooring T data @ 1020m [data set]. https://doi.org/10.71761/cf62771e-39d4-459c-81cc-1469f51a1516, 2026o.

Pearlman, J., Bushnell, M. Coppola, L., Karstensen, J., Buttigieg, P. L., Pearlman, F., Simpson, P., Barbier, M., Muller-Karger, F. E. et al.: Evolving and Sustaining Ocean Best Practices and Standards for the Next Decade. Frontiers in Marine Science, 6:277, 19. https://doi.org/10.3389/fmars.2019.00277, 2019.

Polyakov, I. V., Pnyushkov, A. V., Alkire, M. B., Ashik, I. M., Baumann, T. M., Carmack, E. C., Goszczko, I., Guthrie, J., Ivanov, V. V., Kanzow, T., Krishfield, R., Kwok, R., Sundfjord, A., Morison, J., Rember, R., & Yulin, A.: Greater role for Atlantic inflows on sea-ice loss in the Eurasian Basin of the Arctic Ocean. Science, 356(6335), 285–291. https://doi.org/10.1126/science.aai8204, 2017.

Repp, K.: The hydrology of Bayelva, Spitsbergen. Nord. Hydrol., 19 (4), 259-268, 1988.

Richter-Menge J, Osborne E, Druckenmiller M and Jeffries M O (ed) 2019 The Arctic [in 'State of the Climate in 2018'] Bull. Am. Meteorol. Soc. 100 S 141–68.

Rudels, B.: The thermohaline circulation of the Arctic Ocean and the Greenland Sea. Philosophical Transactions of the Royal Society A, 352, 287–299, 1995.

Rudels, B.: Arctic Ocean Circulation. Encyclopedia of Ocean Sciences, 211–225. https://doi.org/10.1016/B978-012374473-9.00601-9, 2009.

Sanchez-Vidal, A., Veres, O., Langone, L., Ferre, B., Calafat, A., Canals, M., de Madron, X.D., Heussner, S., Mienert, J., Grimalt, J.O., Pusceddu, A., Danovaro, R.: Particle sources and downward fluxes in the eastern Fram strait under the influence of the west Spitsbergen current. Deep-Sea Res. Part I-Oceanogr. Res. Pap. 103 (0), 49–63, https://doi.org/10.1016/j.dsr.2015.06.002, 2015.

Scholzen, C., Schuler, T. V., & Gilbert, A. Sensitivity of subglacial drainage to water supply distribution at the Kongsfjord basin, Svalbard. The Cryosphere, 15(6), 2719–2738. https://doi.org/10.5194/tc-15-2719-2021, 2021.

Serreze M C and Barry R G. Processes and impacts of Arctic amplification: a research synthesis. Glob. Planet. Change 77, (1-2), 85–96, https://doi.org/10.1016/j.gloplacha.2011.03.004, 2011.

Simoncelli, S., Cowley, R., Cheng, L., Dong, S., Parks, J., Storto, A., ... & Kramp, M.: Strengthening the ocean data expert's community for timely and high-quality data provision. Bulletin of the American Meteorological Society, 106(8), E1589-E1600, https://doi.org/10.1175/BAMS-D-25-0143.1, 2025.

Skarðhamar, J. & Svendsen, H.: Short-term hydrographic variability in a stratified Arctic fjord. In: Howe, J. A., Austin, W. E. N., Forwick, M. & Paetzel, M. (eds) Fjord Systems and Archives. Geological Society, London, Special Publications, 344, 51–60, 2010.

Skogseth, R., Olivier, L. L., Nilsen, F., Falck, E., Fraser, N., Tverberg, V., et al.: Variability and decadal trends in the Isfjorden (Svalbard) ocean climate and circulation–an indicator for climate change in the European Arctic. Prog. Oceanogr. 187:102394. doi: 10.1016/j.pocean.2020.10 2394, 2020.

Stigebrandt, A.: Hydrodynamics and circulation of Fjords, in Encyclopedia of Lakes and Reservoirs, edited by L. Bengtsson, R. Herschy, and R. Fairbridge, pp. 327–344, Springer, Netherlands, doi:10.1007/978-1-4020-4410-6_247, 2012.

Straneo, F., & Cenedese, C.: The dynamics of Greenland's glacial fjords and their role in climate. Annual Review of Marine Science, 7(1), 89–112. https://doi.org/10.1146/annurev-marine-010213-135133, 2015.

Svendsen, H., Beszczynska-Møller, A., Hagen, J. O., Lefauconnier, B., Tverberg, V., Gerland, S., et al.: The physical environment of Kongsfjorden–Krossfjorden, an Arctic fjord system in Svalbard. Polar Research, 21(1), 133–166. https://doi.org/10.3402/polar.v21i1.6479, 2002.

Sundfjord, A., Albretsen, J., Kasajima, Y., Skogseth, R., Kohler, J., Nuth, C., et al.: Effects of glacier runoff and wind on surface layer dynamics and Atlantic Water exchange in Kongsfjorden, Svalbard; a model study. Estuarine, Coastal and Shelf Science, 187, 260–272. https://doi.org/10.1016/j.ecss.2017.01.015, 2017.

Szesciorka, A. R., Bensi, M., Giordano, P., Paladini de Mendoza, F., Russo, A., & Giorli, G.: Acoustic evidence of year-round sperm whale foraging, population structure, and sex-specific migration near Svalbard. The Journal of the Acoustical Society of America, 158(3), 1921-1933, 2025.

Tanhua, T., Bulsiewicz, K., & Rhein, M.: Spreading of overflow water from the Greenland to the Labrador Sea. Geophysical Research Letters, 32, L10605. https://doi.org/10.1029/2005GL022700, 2005.

Tanhua T, Pouliquen S, Hausman J, O'Brien K, Bricher P, de Bruin T, Buck JJH, Burger EF, Carval T, Casey KS, Diggs S Giorgetti A, Glaves H, Harscoat V,Kinkade D, Muelbert JH, Novellino A, Pfeil B, Pulsifer PL, Van de Putte A, Robinson E, Schaap D, Smirnov A, Smith N, Snowden D, Spears T, Stall S, Tacoma M, Thijsse P, Tronstad S, Vandenberghe T, Wengren M, Wyborn L and Zhao Z,:Ocean FAIR Data Services. Front. Mar. Sci. 6:440. https://doi.10.3389/fmars.2019.00440, 2019.

Teigen, S. H., F.Nilsen, R.Skogseth, B.Gjevik, and A.Beszczynska-Möller: Baroclinic instability in the West Spitsbergen Current, J. Geophys. Res., 116, C07012, https://doi.10.1029/2011JC006974, 2011.

Tverberg, V., Skogseth, R., Cottier, F., Sundfjord, A., Walczowski, W., Inall, M. E., et al.: The Kongsfjorden transect seasonal and inter-annual variability in hydrography. in the Ecosystem of Kongsfjorden, Svalbard, eds H. Hop and C. Wiencke (Cham: Springer), 49–104. https://doi.10.1007/978-3-319-46425-1_3, 2019.

Walczowski, W., Piechura, J., Osinski, R., Wieczorek, P.: The West Spitsbergen Current volume and heat transport from synoptic observations in summer. Deep-Sea Research Part I 52, 1374–1391 https://10.1016/j.dsr.2005.03.009, 2005.

Wang, H., Zhao, J., Li, F., & Lin, X: Seasonal and interannual variability of the Meridional Overturning Circulation in the subpolar North Atlantic diagnosed from a high-resolution reanalysis data set. Journal of Geophysical Research: Oceans, 126, e2020JC017130. https://doi.org/10.1029/2020JC017130, 2021.

Wilkinson, M. D., Dumontier, M., Aalbersberg, I. J., Appleton, G., Axton, M., Baak, A., et al.: The FAIR guiding principles for scientific data management and stewardship. Sci. Data 3:160018. https://doi.org/10.1038/sdata.2016.18, 2016.

Wobus, F., Shapiro, G., Huthnance, J., & Maqueda, M.: The piercing of the Atlantic Layer by an Arctic shelf water cascade in an idealised study inspired by the Storfjorden overflow in Svalbard', Ocean Modelling, 71, 54-65. https://doi.org/10.1016/j.ocemod.2013.03.003, 2013.

https://doi.org/10.5194/essd-2026-501
Preprint. Discussion started: 22 July 2026

Randall, D., Dazlich, D., Heikes, R., and Konor, C.: CSU model for DCMIP 2016, Zenodo [code], https://doi.org/10.5281/zenodo.5800992018, 2017.

Singh, O. N. and Fabian, P. (Eds.): Atmospheric Ozone: a Millennium Issue, Copernicus Publications, Katlenburg-Lindau, Germany, 147 pp., ISBN 393658608X, 2003.

van Edig, X., Schwarze, S., and Zeller, M.: The robustness of indicator based poverty assessment tools in changing environments – empirical evidence from Indonesia, in: Tropical Rainforests and Agroforests under Global Change, Environmental Science and Engineering (Environmental Engineering), edited by: Tscharntke, T., Leuschner, C., Veldkamp, E., Faust, H., Guhardja, E., and Bidin, A., Springer, Berlin, Heidelberg, Germany, 191–211, https://doi.org/10.1007/978-3-642-00493-3_9, 2010.